Available online at www.sciencedirect.com
SCIENCE DIRECT®
Lithos 74 (2004) 199–232
LITHOS
www.elsevier.com/locate/lithos

Crustal contamination of mafic magmas: evidence from a petrological, geochemical and Sr–Nd–Os–O isotopic study of the Proterozoic Isortoq dike swarm, South Greenland

Ralf Halama[a], Michael Marks[a], Gerhard Brügmann[b], Wolfgang Siebel[a], Thomas Wenzel[a], Gregor Markl[a,*]

[a] *Institut für Geowissenschaften, Eberhard-Karls-Universität Tübingen, Wilhelmstrasse 56, D-72074 Tübingen, Germany*
[b] *Max-Planck-Institut für Chemie, Abteilung Geochemie, Postfach 3060, D-55020 Mainz, Germany*

Received 10 June 2003; accepted 10 March 2004

Available online 27 April 2004

Abstract

The mid-Proterozoic Isortoq dike swarm in the Gardar Province, South Greenland, comprises a variety of alkaline rocks ranging from gabbroic to syenitic in composition. Major magmatic mineral phases are olivine, clinopyroxene, Fe–Ti oxides, amphibole, plagioclase and alkali feldspar. Quartz occurs in some samples as a late magmatic phase. Liquidus temperatures of olivine-bearing samples range between 1120 and 1145 °C and solidus temperatures are 850–930 °C. Calculated silica activities are highly variable between 0.53 and unity. Oxygen fugacities vary from −3 to +1 log units relative to the fayalite–magnetite–quartz buffer.

The rocks have MgO contents <6 wt.% with Mg# between 53 and 17. Primitive mantle-normalized trace element patterns show a relative enrichment of LIL elements with Ba peaks and Nb troughs. Clinopyroxenes show a general enrichment in REE relative to chondritic values with variable slightly positive to prominent negative Eu anomalies. Two of the dikes were dated with Sm–Nd three-point isochrons at 1190 ± 44 and 1187 ± 87 Ma, respectively. Initial $^{87}Sr/^{86}Sr$ ratios of mafic mineral separates range from 0.70289 to 0.70432 and initial ε_{Nd} values vary from +0.3 to −10.7. Whole-rock initial $^{187}Os/^{188}Os$ ratios are highly variable including very radiogenic values of up to 7.967. $\delta^{18}O_{v\text{-}smow}$ values of separated clinopyroxene and amphibole range from +5.2 ‰ to +6.2 ‰ and fall within the range of typical mantle-derived rocks, although mixing with a lower crustal component is permitted by the data. Using energy-constrained assimilation-fractional crystallization (EC-AFC) modeling equations, the Sr–Nd isotope data of the more radiogenic samples can successfully be modeled by addition of up to 10% lower crustal granulite-facies Archean gneisses as contaminants. The Os isotopic data also suggest the involvement of old radiogenic crust. In accordance with seismic data, we conclude that a wedge of Archean crust extends from West Greenland further to the south below the present erosion level.

Keywords: Sr–Nd–Os–O isotopes; QUILF; EC-AFC modeling; Mafic dike swarm; Gardar province; South Greenland

1. Introduction

Mafic dike swarms of Proterozoic age are widespread in many Precambrian cratons and their intru-

* Corresponding author. Tel.: +49-7071-2972930.
E-mail address: markl@uni-tuebingen.de (G. Markl).

0024-4937/$ - see front matter © 2004 Elsevier B.V. All rights reserved.
doi:10.1016/j.lithos.2004.03.004

sion indicates a considerable extension of the continental crust (Tarney and Weaver, 1987). Studies of rift-related mafic dike swarms are essential for understanding generation of such extensive mafic magmatism, and they may be used to identify mantle plumes (Ernst and Buchan, 1997, 2001). There is general agreement that mafic mantle-derived magmas experience some degree of crustal contamination during ascent and/or residence in crustal magma chambers (Mohr, 1987). The crust is both a density filter and a source of incompatible elements (Lightfoot et al., 1991) and it may act as a site of extensive and extensive partial crystallization of primitive melts (O'Hara and Herzberg, 2002). However, there is much debate whether the trace element and isotopic characteristics of intracontinental basalts are mantle-derived or due to crustal contamination. Crustal contamination has been shown to be important in the petrogenesis of flood basalts (Devey and Cox, 1987; Peng et al., 1994; Chesley and Ruiz, 1998; Baker et al., 2000). On the other hand, a mantle source enriched in incompatible trace elements not influenced by a major crustal input was postulated for some Proterozoic dike swarms (Tarney and Weaver, 1987; Condie et al., 1987; Boily and Ludden, 1991) and other flood basalts (Molzahn et al., 1996). If a mantle-derived geochemical signature can be demonstrated, it remains difficult to locate the mantle source, i.e., whether the magmas are predominantly derived from the subcontinental lithospheric mantle (SCLM) (e.g., Gallagher and Hawkesworth, 1992; Turner et al., 1996), from an upwelling mantle plume (e.g., LeCheminant and Heaman, 1989; Walker et al., 1997; Puchtel et al., 1999) or from a mixture of both (e.g., Ellam et al., 1992; Gibson et al., 1995; Thompson et al., 1998).

Here we present new petrological, geochemical and isotopic data of the Isortoq dike swarm in the mid-Proterozoic igneous Gardar Province in South Greenland. The Gardar Province represents a failed rift and comprises numerous mafic dikes of different generations. The Isortoq dike swarm is one major Gardar mafic dike swarm which has not been studied in great detail before, although the feldspathic inclusions in some of the dikes were the topic of several investigations (Bridgwater, 1967; Bridgwater and Harry, 1968; Halama et al., 2002). Because the swarm comprises a variety of petrographically diverse dike rocks ranging from gabbroic to syenitic in composition, it is well suited to study the influence of crustal assimilation processes on the composition of intracontinental mafic magmas. For that purpose, we combine petrological with Sr–Nd–O isotopic and whole-rock geochemical data. Additionally, we apply the Re–Os method which is known to have a great potential as tracer of crustal contamination (e.g., Chesley and Ruiz, 1998). The olivine–gabbroic dikes may provide information on the nature of the mantle sources for the dikes and Gardar magmatism in general.

2. Geological setting

The mid-Proterozoic Gardar Province in South Greenland represents a rift-related igneous province with magmatic activity lasting from about 1.35 to 1.14 Ga (Emeleus and Upton, 1976; Upton and Emeleus, 1987; Upton et al., 2003) (Fig. 1a). The country rocks mainly consist of I-type calc-alkaline granitoids (Julianehåb batholith) of Early Proterozoic age (van Bremen et al., 1974; Allaart, 1976; Patchett and Bridgwater, 1984; Kalsbeek and Taylor, 1985). Recent work (Garde et al., 2002) indicates that the Julianehåb batholith was emplaced mainly between 1.85 and 1.80 Ga. In the northwestern part of the province, Archean rocks of the Border and Foreland Zones of the craton comprise the basement (Allaart, 1976). Apart from 12 major alkaline igneous complexes and a succession of supracrustal lavas and sediments (Eriksfjord Formation), a large number of dike rocks with variable chemical composition intruded the basement. Two major dike swarms were emplaced into the Julianehåb batholith along WSW–ENE to SW–NE trends in the Tugtutôq–Ilímaussaq and the Nunarssuit–Isortoq zones during the late Gardar period (~ 1.20–1.14 Ga). The latter of these is the topic of the present paper.

In the Isortoq area, several generations of gabbroic to intermediate dikes with variable widths from a few centimeters to several hundred meters occur (Bridgwater and Coe, 1970, Fig. 1b). The earliest generation of Gardar dikes belongs to a regional dike swarm of early-Gardar olivine dolerites ("Brown Dikes" or "BD_0 dikes") trending WNW–ESE across the Gardar province. They are dated at

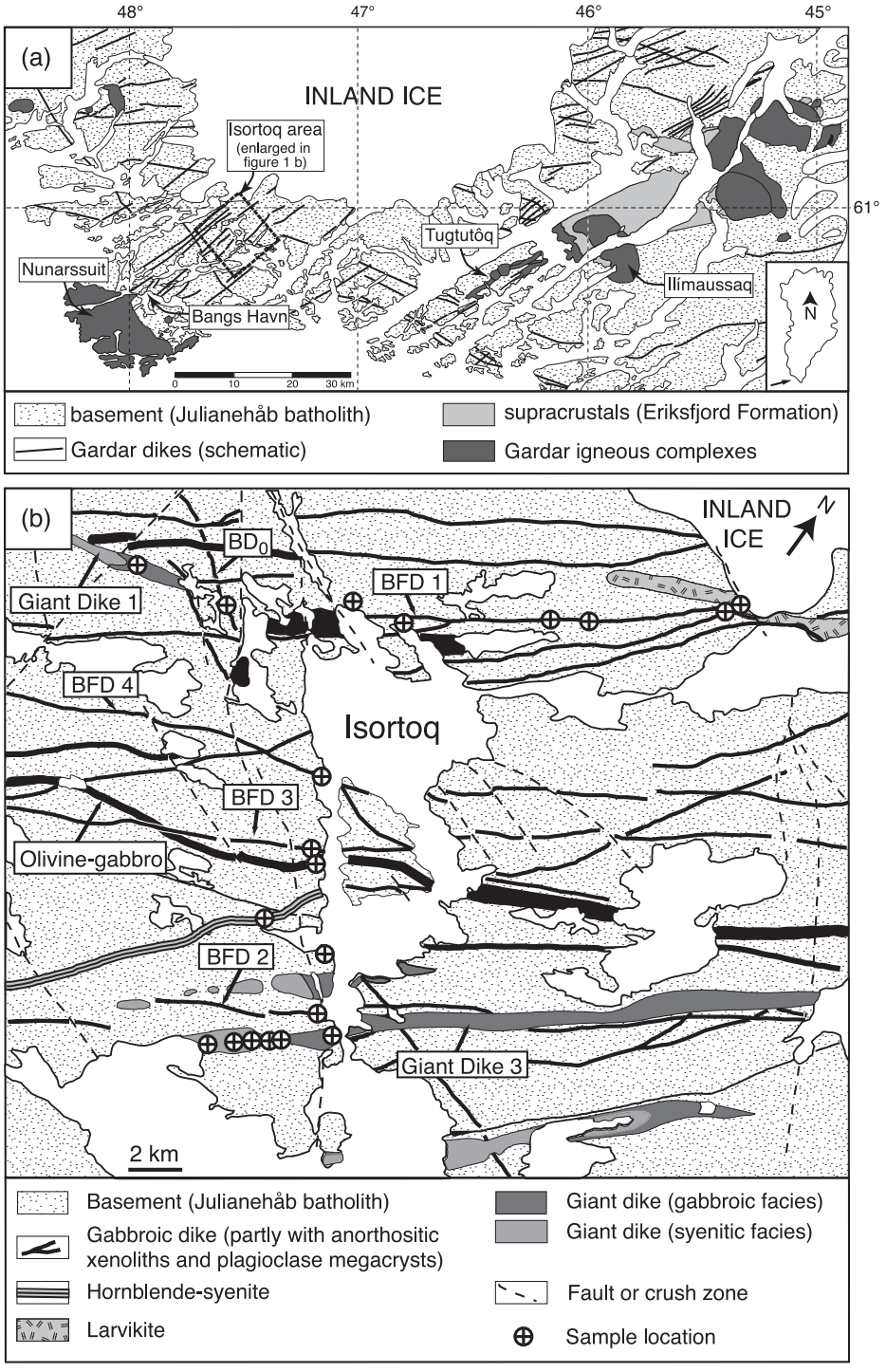

Fig. 1. (a) Map of the Gardar Province (after Upton and Emeleus, 1987). (b) Map of the Isortoq region (after Bridgwater and Coe, 1970) with sample localities.

1282 ± 5 Ma (Upton et al., 2003), predating the main late-Gardar dike swarm of the Isortoq area. The late-Gardar dikes of the Nunarssuit–Isortoq region were emplaced along WSW–ENE to SW–NE trends. The most spectacular feature of the dike swarm is the abundance of anorthosite xenoliths and feldspar megacrysts in some of the gabbroic dikes (Bridgwater and Harry, 1968; Halama et al., 2002) that are informally named "Big Feldspar Dikes" (BFDs). The feldspathic material varies from single feldspar crystals (< 1 cm to 1 m in size) to anorthositic bodies up to 30 m long. It is considered as evidence for an anorthosite body underlying South Greenland (Bridgwater, 1967). BFD 1 can be traced for 30 km and is one of the dikes with the greatest volume of feldspathic material in South Greenland (Bridgwater and Harry, 1968). BFD 2 is a composite dike that consists of a 1–2-m-wide marginal microsyenite enclosing a feldspathic alkaline gabbro (Bridgwater and Harry, 1968). The amount of feldspathic material is about average in BFD 3, but relatively low in BFD 4. Olivine–gabbros without excessive feldspathic material but with a similar trend as the BFDs also occur. Composite dikes comprising a gabbroic, a syenitic and an intermediate syeno-gabbroic facies with maximum widths of up to 500 m are called "Giant Dikes". They postdate all other members of the swarm (Bridgwater and Coe, 1970) and represent a connecting link between the mafic dykes and the major intrusions of the Gardar province. Giant Dike 3 is the least altered of the Giant Dikes and was therefore selected for a detailed study. Two further, petrographically distinct dikes investigated in this study include a larvikite and a hornblende–syenite.

3. Analytical methods

Mineral compositions were determined using a JEOL 8900 electron microprobe at the Institut für Geowissenschaften, Universität Tübingen, Germany. An internal $\varphi\rho Z$ correction of the raw data was applied (Armstrong, 1991). Both synthetic and natural standards were used. Measuring times were 16 s for major elements and 30 s for minor elements. The emission current was 15 nA and the acceleration voltage 15 kV. For feldspar analyses, a beam diameter of 5 μm was used to avoid Na migration. The bulk compositions of oxy-exsolved titanomagnetite grains were reconstructed by combining image processing (NIH Image software) of backscattered electron images of the exsolved grains with point analyses of exsolved ilmenite and broad beam analyses of exsolved magnetite (Marks and Markl, 2001).

Rare earth element (REE) contents in clinopyroxenes were measured by in situ laser ablation inductively coupled plasma-mass spectrometry (LA-ICP-MS) at the EU Large-Scale Geochemical Facility (University of Bristol) using a VG Elemental PlasmaQuad 3 + S-Option ICP-MS equipped with a 266 nm Nd-YAG laser (VG MicroProbe II). Details of the method are described by Halama et al. (2002). The precision of trace element concentrations, based on repeated analyses of standards, is approximately ± 5% for element concentrations >10 ppm and ± 10% for concentrations < 10 ppm. Typical detection limits for the REE in this study were 0.04–0.6 ppm.

Whole-rock analyses were performed by standard X-ray fluorescence (XRF) techniques at the Universität Mainz, using a Philips PW 1404 spectrometer and at the Universität Freiburg, using a Philips PW 2404 spectrometer. Pressed powder pellets and fused glass discs were prepared to measure contents of trace and major elements, respectively. The raw data were processed with the standard XR-55 software of Philips. Natural standards were used for calibration. Detection limits vary between 1 and 10 ppm, depending on the specific trace element and on the instrument used.

For Sr and Nd isotope analyses, about 10 mg of hand-picked mineral separate was spiked with mixed ^{84}Sr–^{87}Rb and ^{150}Nd–^{149}Sm tracers before dissolution under high pressure in HF at 180 °C in polytetrafluorethylene reaction bombs. Rb, Sr, Sm and Nd were separated and measured as described by Marks et al. (2003). Analyses of the Ames Nd standard (Geological Survey of Canada, Roddick et al., 1992) gave $^{143}Nd/^{144}Nd = 0.512119 \pm 10$ ($\pm 2\sigma$, $n = 42$) and analyses of the NBS 987 Sr standard yielded $^{87}Sr/^{86}Sr = 0.710261 \pm 16$ ($\pm 2\sigma$, $n = 30$). $^{143}Nd/^{144}Nd$ ratios were cross-checked with the La Jolla Nd standard which gave 0.511831 ± 30 ($\pm 2\sigma$, $n = 12$). ε_{Nd} values were calculated using present-day CHUR values of 0.1967 for $^{147}Sm/^{144}Nd$ (Jacobson and Wasserburg, 1980) and 0.512638 for $^{143}Nd/^{144}Nd$ (Goldstein et al., 1984). The

uncertainty in ε_{Nd} based on analytical errors is less than $0.5\varepsilon_{Nd}$ units.

For Re–Os isotope analyses, 2–3 g of bulk sample powder was dissolved and equilibrated with a ^{185}Re–^{190}Os mixed spike using aqua regia digestion in sealed Carius tubes (Shirey and Walker, 1998). Details of the further analytical procedures based on the method of Birck et al. (1997) are described by Puchtel et al. (2001). Re and Os isotopic compositions were measured via negative thermal ionization mass spectrometry at the MPI für Chemie at Mainz. Effects of mass fractionation were eliminated by normalizing to $^{192}Os/^{188}Os = 3.082678$. Re isotopic ratios were not corrected for fractionation. Analytical errors were determined by multiple analyses of internal MPI standards. They are ± 0.5% on both Os isotopic composition and Re/Os ratio. Initial $^{187}Os/^{188}Os$ ratios were calculated using the ^{187}Re decay constant of 1.666×10^{-11} a^{-1} (Shirey and Walker, 1998).

Oxygen isotope compositions of powdered whole-rock basement samples were determined by a conventional method modified after Clayton and Mayeda (1963) and Vennemann and O'Neil (1993), using BrF_5 as reagent and converting the liberated oxygen to CO_2. The oxygen isotope composition of 0.5–2 mg handpicked mineral separates was determined using a laser fluorination method adapted after Sharp (1990) and Rumble and Hoering (1994). Details of the method are described by Marks et al. (2003). Results are given in the standard δ notation, expressed relative to V-SMOW in per mil (‰). Replicate oxygen isotope analyses of the NBS-28 quartz standard had an average precision of ± 0.1‰ for $\delta^{18}O$. In each run, standards were analyzed at the beginning and the end of the sample set. A correction was applied to the data equal to the average of the difference between the mean measured value and the accepted value for the standard (9.64‰).

Table 1
Sample description

Dike	Type	Sample	Ol	Cpx	Feldspar	Amph	Qtz	Fe–Ti oxides
BD_0	gabbro	GD 37	⊕	⊕	plag			mag
BFD 1	gabbro	GM 1680	⊕	⊕	plag			mag
	plagioclase megacryst	GM 1681		⊕	plag			
	anorthosite xenolith	GM 1682		⊕	plag	±	±	mag
	gabbro	GM 1729	⊕	⊕	plag			
	gabbro	GM 1735	⊕	⊕	plag			mag
BFD 2	leucogabbro from the dike center	GM 1750		⊕	plag		±	mag
BFD 3	gabbro	GM 1805	⊕	⊕	plag			mag
BFD 4	gabbro	GD 39	⊕	⊕	plag			ilm + mag
Olivine–gabbro	gabbro	GM 1803	⊕	⊕	plag			mag
Giant Dike 1	syeno-gabbro	GM 1712		⊕	plag + alk			mag
Giant Dike 3	sample traverse from center to margin in gabbroic facies	GM 1759–1762	⊕	⊕	plag + alk			ilm + mag
	syenite	GM 1768		⊕	alk	±		mag
	sample traverse from margin to margin in syenitic facies	GM 1769–1776		⊕	alk	±		mag
	syenite	GM 1778		⊕	alk	±		mag
	syenite	GM 1780		⊕	alk	±		mag
	syenite	GM 1784		⊕	alk	±		mag
Larvikite	larvikite from the dike center	GM 1684	⊕	⊕	plag + alk	±	±	ilm + mag
Hornblende–syenite	syenite	GD 38			alk	⊕	⊕	mag

Mineral is a major component of the sample (⊕), minor amounts of mineral present (±).

4. Results

4.1. Petrography

Major mineral assemblages of the samples investigated in this study are summarized in Table 1. Abbreviations used there and in text and figures are after Kretz (1983).

4.1.1. Olivine–gabbro and "big feldspar dikes" (BFDs)

The major magmatic mineral phases in the olivine–gabbro and in BFDs 1, 3 and 4 are subhedral olivine, plagioclase and interstitial clinopyroxene. The excessive feldspathic material characteristic of the BFDs is absent in the olivine–gabbro, but otherwise, both rock types are petrographically very similar. In BFD 2, olivine is lacking, but some quartz occurs interstitially. Minor phases are apatite, Fe–Ti oxides and sulphides. Biotite is fairly common and can occur either as single grain or surrounding Fe–Ti oxides or olivine. Titanite, amphibole and chlorite occur as secondary alteration products.

4.1.2. Giant Dikes

The Giant Dikes consist of a gabbroic and a syenitic facies. In the gabbroic samples, primary minerals are plagioclase, alkali feldspar, anhedral olivine, interstitial clinopyroxene, titanomagnetite, ilmenite, and in some samples high amounts of apatite. In two samples (GM1761 and GM1762), olivine is rimmed by a second clinopyroxene generation. Biotite and/or chlorite overgrow olivine, clinopyroxene and Fe–Ti oxides, whereas amphibole is absent. The transition from the gabbroic to the syenitic facies is characterized by the disappear-

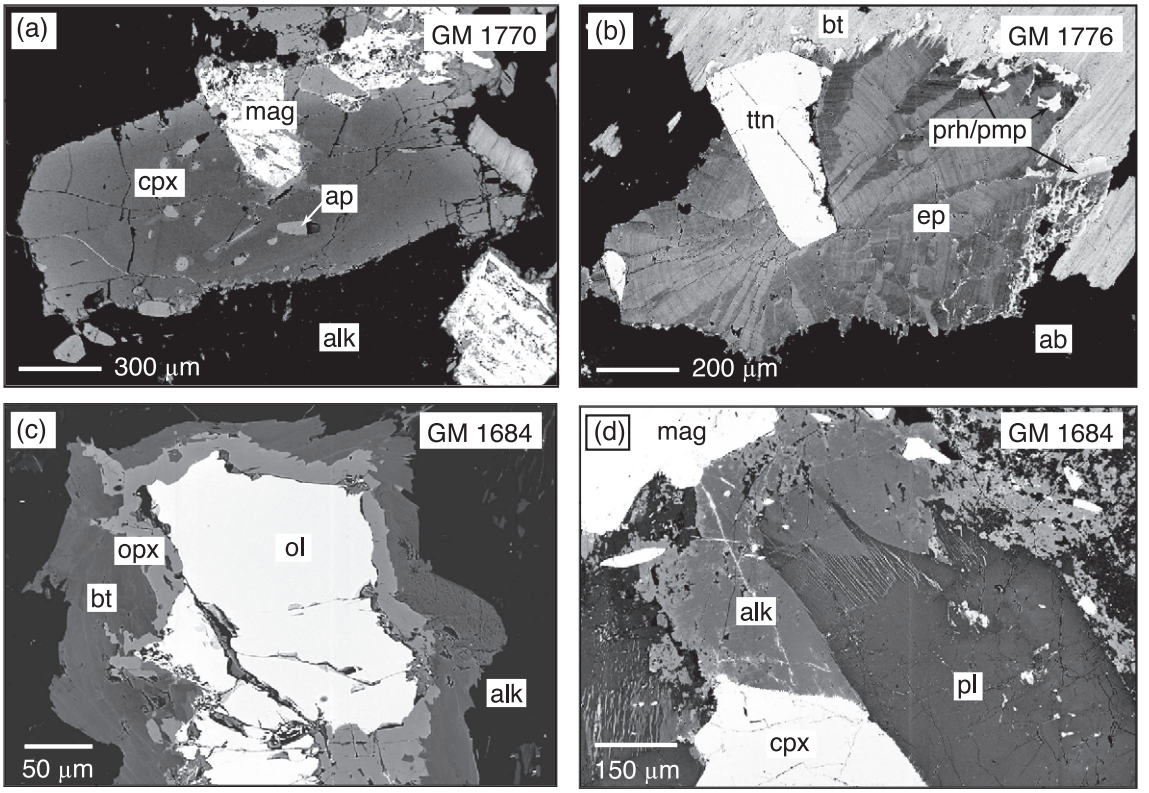

Fig. 2. Backscattered electron (BSE) images of (a) euhedral clinopyroxene with apatite inclusions in the gabbroic facies of Giant Dike 3, (b) sector-zoned epidote associated with titanite, biotite, albite, pumpellyite and prehnite in the syenitic facies of Giant Dike 3, (c) olivine, overgrown by orthopyroxene and biotite, in the larvikite and (d) plagioclase surrounded by alkali feldspar in the larvikite.

ance of plagioclase, olivine and primary ilmenite, and the abundant occurrence of amphibole. Additionally, clinopyroxene in syenitic samples is euhedral to subhedral but never occurs as interstitial grains (Fig. 2a). As in the gabbroic samples, primary titanomagnetite is oxy-exsolved to ilmenite and magnetite. The exsolved ilmenite laths are selectively altered to titanite and chlorite. Most oxide grains are rimmed by amphibole, biotite and chlorite. In all syenitic samples, aggregates of sector-zoned epidote, associated with titanite, biotite and interstitial albite can be observed (Fig. 2b). In some places, pumpellyite and prehnite occur as breakdown products of epidote. Sample GM1712 from the Giant Dike 1 is intermediate between the two abovementioned facies. Primary olivine is strongly altered, titanomagnetite is the only primary Fe–Ti oxide, but plagioclase is still present in this sample.

4.1.3. Larvikite

In the larvikite, olivine is very rare, and is surrounded by orthopyroxene (Fig. 2c). The major magmatic phases are clinopyroxene, plagioclase and alkali feldspar. Plagioclase is less common than alkali feldspar and is rimmed by the latter (Fig. 2d). Accessory phases in the larvikite include euhedral to subhedral amphibole, interstitial quartz, biotite, apatite, Fe–Ti oxides and sulphides. Secondary talc, titanite and chlorite are relatively rare.

Table 2
Representative microprobe analyses of feldspar from Isortoq dike rocks

Dike	Olivine–gabbro	BFD 2	BFD 2	GD 3 gabbro	GD 3 gabbro	GD 3 gabbro	GD 3 gabbro	GD 3 gabbroc	GD 3 gabbro	GD 3 syenite	GD 3 syenite	Larvikite	Larvikite	Larvikite
Sample	GM 1803	GM 1750	GM 1749	GM 1760	GM 1760	GM 1761	GM 1762	GM 1762	GM 1762	GM 1774	GM 1774	GM 1684	GM 1684	GM 1684
wt.%														
SiO_2	53.87	56.49	62.81	62.88	62.55	56.01	65.35	64.84	62.73	65.17	64.20	57.16	62.42	64.41
TiO_2	0.25	0.08	0.05	0.04	0.05	0.05	0.01	0.00	0.05	0.07	0.01	0.08	0.12	0.03
Al_2O_3	27.78	26.46	21.92	22.50	21.98	27.66	19.10	19.88	22.76	19.42	19.11	26.05	21.52	20.00
FeO	1.66	0.51	0.24	0.25	0.27	0.17	0.13	0.11	0.10	0.14	0.11	0.35	0.36	0.19
MnO	0.04	0.00	0.01	0.00	0.00	0.00	0.02	0.02	0.05	0.00	0.00	0.00	0.00	0.02
MgO	0.56	0.08	0.01	0.03	0.00	0.02	0.00	0.00	0.00	0.01	0.00	0.03	0.01	0.01
BaO	0.00	0.05	0.41	0.17	0.23	0.04	0.08	0.12	0.06	0.28	1.59	0.20	0.93	0.77
SrO	0.23	0.25	0.20	0.31	0.29	0.32	0.12	0.16	0.37	0.21	0.24	0.21	0.21	0.20
CaO	9.88	9.86	4.09	3.94	3.55	9.47	0.57	1.43	4.34	0.85	0.31	8.29	3.04	1.51
Na_2O	4.23	5.49	6.43	7.93	6.16	5.46	4.01	4.94	8.24	6.58	4.12	6.61	7.33	5.84
K_2O	0.93	0.70	3.88	1.95	4.72	0.38	10.61	8.37	0.89	6.76	10.03	0.40	3.33	6.83
Total	99.42	99.97	100.04	99.99	99.79	99.60	99.99	99.89	99.60	99.50	99.72	99.39	99.27	99.82
Formulae based on eight oxygens														
Si	2.46	2.55	2.82	2.81	2.83	2.53	2.97	2.94	2.80	2.95	2.96	2.59	2.83	2.92
Al	1.50	1.41	1.16	1.18	1.17	1.47	1.02	1.06	1.20	1.04	1.04	1.39	1.15	1.07
Ti	0.01	0.00	0.00	0.00	0.00	0.00	0.00	0.00	0.00	0.00	0.00	0.00	0.00	0.00
Fe^{2+}	0.06	0.02	0.01	0.01	0.01	0.01	0.00	0.00	0.00	0.01	0.00	0.01	0.01	0.01
Mn	0.00	0.00	0.00	0.00	0.00	0.00	0.00	0.00	0.00	0.00	0.00	0.00	0.00	0.00
Mg	0.04	0.01	0.00	0.00	0.00	0.00	0.00	0.00	0.00	0.00	0.00	0.00	0.00	0.00
Ba	0.00	0.00	0.01	0.00	0.00	0.00	0.00	0.00	0.00	0.01	0.03	0.00	0.02	0.01
Sr	0.01	0.01	0.01	0.00	0.00	0.00	0.00	0.00	0.00	0.00	0.00	0.01	0.01	0.01
Ca	0.48	0.48	0.20	0.19	0.17	0.46	0.03	0.07	0.21	0.04	0.02	0.40	0.15	0.07
Na	0.38	0.48	0.56	0.69	0.54	0.48	0.35	0.43	0.71	0.58	0.37	0.58	0.64	0.51
K	0.05	0.04	0.22	0.11	0.27	0.02	0.62	0.48	0.05	0.39	0.59	0.02	0.19	0.39
Total	4.99	5.00	4.99	5.00	4.99	4.98	5.00	4.99	4.98	5.01	5.00	5.01	5.01	5.00
X_{an}	0.53	0.48	0.20	0.19	0.17	0.48	0.03	0.07	0.21	0.04	0.02	0.40	0.15	0.07
X_{ab}	0.41	0.48	0.57	0.70	0.55	0.50	0.35	0.44	0.73	0.57	0.38	0.58	0.65	0.52
X_{Or}	0.06	0.04	0.23	0.11	0.28	0.02	0.62	0.49	0.05	0.39	0.61	0.02	0.20	0.40

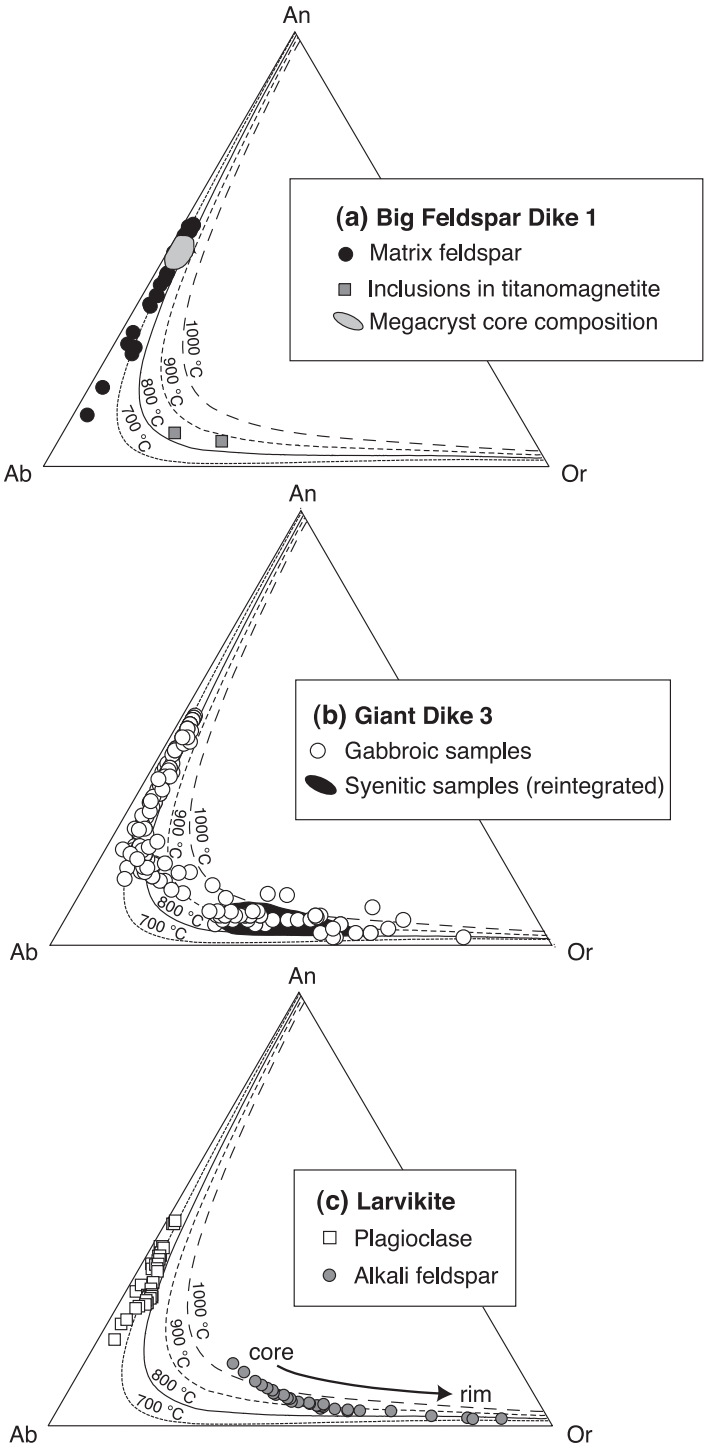

Fig. 3. Feldspar compositions of Isortoq dike rocks in the An–Ab–Or triangle with solvus isotherms after Elkins and Grove (1990).

4.1.4. Hornblende–syenite

Major minerals of this dike rock are euhedral amphibole, alkali feldspar and quartz. Accessory phases are Fe–Ti oxides, biotite, apatite and zircon. Occasional chlorite and titanite are probably of secondary origin.

4.2. Mineral chemistry

4.2.1. Feldspars

Representative feldspar analyses are presented in Table 2 and illustrated in Fig. 3. In the olivine–gabbro and the BFDs, plagioclase is normally zoned and its composition varies between $An_{63}Ab_{36}Or_2$ and $An_{12}Ab_{85}Or_3$ (Fig. 3a). Plagioclase megacryst data from BFDs and the anorthosite xenoliths have been presented in Halama et al. (2002).

The gabbroic samples of Giant Dikes contain plagioclase evolving from $An_{59}Ab_{36}Or_5$ to $An_{15}Ab_{73}Or_{11}$ and alkali feldspar with compositions between $An_{14}Ab_{43}Or_{42}$ and $An_6Ab_{27}Or_{67}$ (Fig. 3b). Maximum anorthite content decreases from the margin to the center of the Giant Dike. In the syenitic facies, plagioclase is lacking, and alkali feldspar composition varies between $An_7Ab_{65}Or_{29}$ to $An_2Ab_{38}Or_{61}$ (Fig. 3b).

The larvikite contains plagioclase ($An_{47}Ab_{51}Or_2$ to $An_{20}Ab_{77}Or_3$) and alkali feldspar ($An_{14}Ab_{56}Or_{30}$ to $An_3Ab_{30}Or_{67}$; Fig. 3c). Large areas of alkali feldspar in the larvikite, and all feldspar in the hornblende–syenite are completely exsolved to albite and orthoclase.

4.2.2. Olivine

Typical olivine analyses are presented in Table 3. Olivine ranges in composition from Fo_{70} to Fo_{32}, with the most Fo-rich olivine in some BFD samples and the most Fa-rich ones in the larvikite (Fig. 4). In the olivine–gabbro and the BFD samples, the compositional variability can reach 20 mol% Fo within a single grain and can be as large as in the whole sample. Some grains show growth zoning patterns

Table 3
Representative microprobe analyses of olivine from Isortoq dike rocks

Dike	Olivine–gabbro	Olivine–gabbro	BFD 1	BFD 1	BFD 4	Giant Dike 3 gabbro	Giant Dike 3 gabbro	Giant Dike 3 gabbro	Larvikite	Larvikite
Sample	GM 1803	GM 1803	GM 1735	GM 1729	GD 39	GM 1759	GM 1761	GM 1760	GM 1684	GM 1684
wt.%										
SiO_2	36.26	33.82	37.16	33.55	35.28	33.28	35.42	34.64	32.89	32.88
TiO_2	0.06	0.07	0.03	0.02	0.02	0.05	0.02	0.01	0.02	0.08
Al_2O_3	0.01	0.01	0.10	0.05	0.02	0.01	0.00	0.00	0.01	0.00
NiO	0.03	0.03	0.06	0.03	0.03	–	–	–	0.00	0.05
FeO	33.23	47.09	29.32	48.71	39.67	48.28	37.72	42.61	52.13	51.03
MnO	0.44	0.91	0.25	0.84	0.71	0.53	0.23	0.65	1.24	1.14
MgO	29.92	17.84	32.67	16.82	24.00	17.00	26.51	21.86	14.05	15.15
CaO	0.25	0.51	0.24	0.19	0.36	0.40	0.33	0.38	0.06	0.09
Total	100.20	100.28	99.82	100.20	100.10	99.55	100.23	100.15	100.40	100.42
Formulae based on four oxygens										
Si	1.00	1.00	1.00	1.00	1.00	1.00	0.99	1.00	1.00	0.99
Al	0.00	0.00	0.00	0.00	0.00	0.00	0.00	0.00	0.00	0.00
Ti	0.00	0.00	0.00	0.00	0.00	0.00	0.00	0.00	0.00	0.00
Mg	1.22	0.79	1.31	0.75	1.02	0.76	1.11	0.94	0.64	0.68
Fe	0.76	1.17	0.66	1.22	0.94	1.21	0.89	1.03	1.33	1.29
Mn	0.01	0.02	0.01	0.02	0.02	0.01	0.01	0.02	0.03	0.03
Ni	0.00	0.00	0.00	0.00	0.00	–	–	–	0.00	0.00
Ca	0.01	0.02	0.01	0.01	0.01	0.01	0.01	0.01	0.00	0.00
Sum	3.00	3.00	3.00	3.00	3.00	3.00	3.01	3.00	3.00	3.00
X_{Fo}	0.614	0.400	0.663	0.380	0.516	0.383	0.553	0.475	0.324	0.346
X_{Fa}	0.383	0.592	0.334	0.617	0.478	0.610	0.442	0.519	0.675	0.653
X_{La}	0.004	0.008	0.004	0.003	0.006	0.006	0.005	0.006	0.001	0.001

Not determined (–).

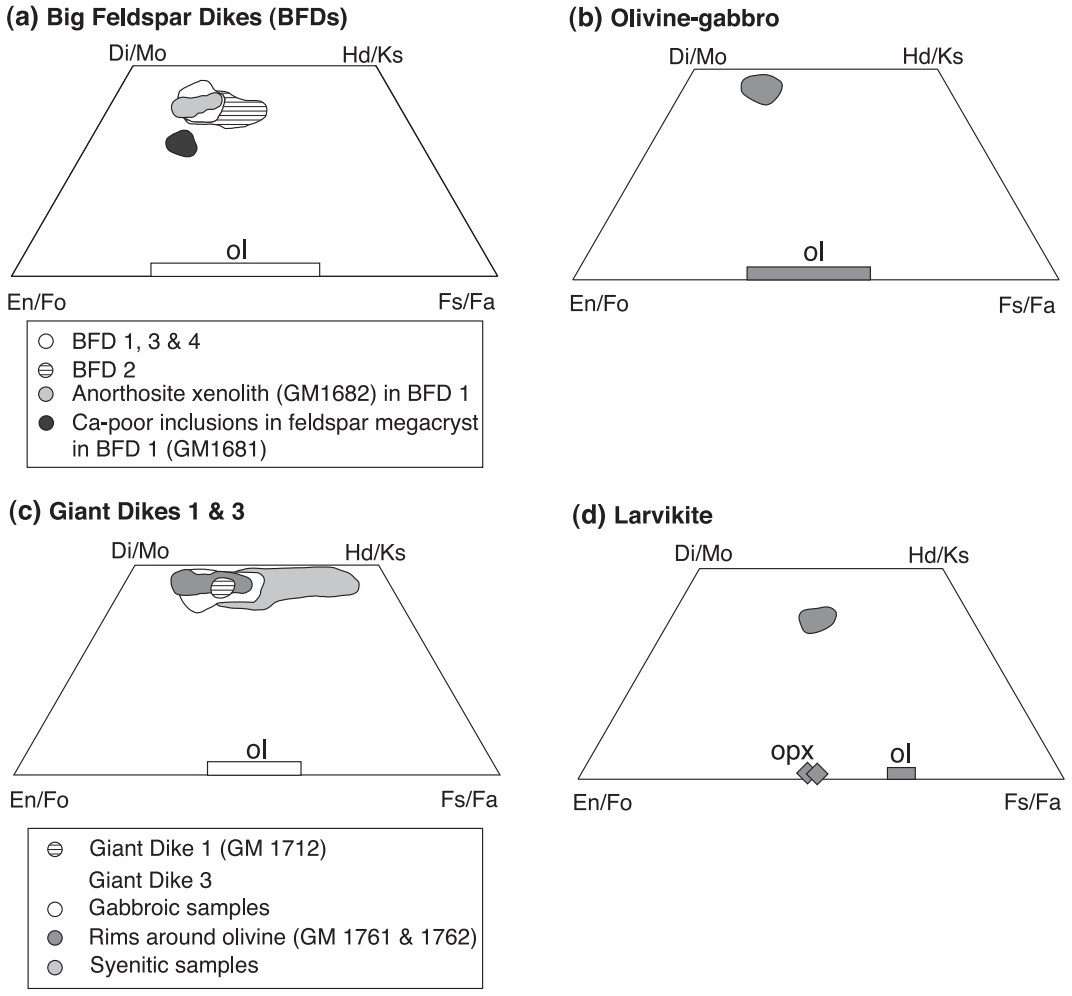

Fig. 4. Olivine and pyroxene compositions of Isortoq dike rocks in the enstatite–ferrosilite–hedenbergite–diopside (En–Fs–Hd–Di) quadrilateral. Fo = forsterite, Fa = fayalite, Ks = kirschsteinite ($CaFeSiO_4$) and Mo = monticellite ($CaMgSiO_4$).

with a decrease in Fo content towards the rims, but most are irregularly zoned. Olivines from Giant Dike 3 and from the larvikite are rather homogeneous with only minor chemical variation within one single grain and sample. In the gabbroic samples of Giant Dyke 3, Fo-contents of olivine decrease systematically from the margin (Fo_{57}) to the center (Fo_{38}) of the dike.

4.2.3. Clinopyroxene

Clinopyroxene of the whole sample suite is subcalcic augite with generally >90% quadrilateral (Di + Hed + En + Fs) components. End-member components are calculated after Lindsley (1983) and some typical analyses are presented in Table 4. Aegirine contents in all samples range from 2 to 10 mol%.

Augites in the olivine–gabbro, the BFDs and the matrix of the anorthosite xenoliths have all similar compositions between $En_{43}Fs_{15}Wo_{42}$ and $En_{30}Fs_{31}Wo_{39}$ (Fig. 4a and b). Some rare augite inclusions in feldspar megacrysts are relatively Ca-poor with a compositional range from $En_{51}Fs_{19}Wo_{31}$ to $En_{48}Fs_{19}Wo_{33}$ (Fig. 4a).

Augite in the gabbroic samples of the two Giant dikes is essentially unzoned and shows a relatively

Table 4
Representative microprobe analyses of pyroxene from Isortoq dike rocks

Dike	Olivine–gabbro	BFD 1	BFD 1	BFD 2	GD 1 syeno-gabbro	GD 3 gabbro	GD 3 gabbro	GD 3 syenite	GD 3 syenite	GD 3 syenite	Larvikite	Larvikite
Sample	GM 1803	GM 1729	GM 1681 Ca-poor inclusion in feldspar	GM 1749	GM 1712	GM 1760	GM 1761 rim around olivine	GM 1769 Fe-rich core	GM 1769 rim	GM 1772	GM 1684 cpx	GM 1684 rim around olivine
wt.%												
SiO_2	51.21	52.49	51.11	51.09	51.18	50.90	53.36	49.92	50.13	49.16	51.59	51.57
TiO_2	1.00	0.37	1.34	0.71	0.99	0.75	0.01	0.88	1.00	0.67	0.70	0.06
Al_2O_3	2.34	1.76	3.15	1.27	0.68	2.21	0.51	0.77	0.92	0.65	0.41	0.36
Cr_2O_3	0.04	0.00	0.00	0.04	0.00	0.02	–	–	–	0.00	0.00	0.00
FeO	9.17	9.56	11.79	17.26	12.62	10.89	8.29	18.91	17.54	22.00	17.30	28.81
MnO	0.17	0.29	0.31	0.53	0.28	0.11	0.10	0.48	0.47	0.51	0.53	0.91
MgO	12.67	13.89	16.35	9.54	11.48	12.71	13.95	6.71	8.02	4.23	11.05	17.41
CaO	22.34	20.87	16.18	19.01	21.35	21.01	22.46	21.50	21.35	21.07	18.19	1.39
Na_2O	0.73	0.56	0.43	0.49	0.42	0.52	0.54	0.40	0.36	0.87	0.32	0.01
Total	99.66	99.80	100.65	99.93	99.01	99.11	99.37	99.58	99.79	99.15	100.08	100.52
Formulae based on four cations and six oxygens												
Si	1.92	1.96	1.88	1.97	1.96	1.93	1.99	1.97	1.95	1.97	1.98	1.98
Al	0.10	0.08	0.14	0.06	0.03	0.10	0.02	0.04	0.04	0.03	0.02	0.02
Ti	0.03	0.01	0.04	0.02	0.03	0.02	0.00	0.03	0.03	0.02	0.02	0.00
Cr	0.00	0.00	0.00	0.00	0.00	0.00	–	–	–	0.00	0.00	0.00
Fe^{3+}	0.06	0.03	0.05	0.00	0.02	0.05	0.04	0.01	0.02	0.06	0.00	0.03
Mg	0.71	0.77	0.90	0.55	0.66	0.72	0.78	0.39	0.47	0.25	0.63	0.99
Fe^{2+}	0.23	0.27	0.31	0.56	0.38	0.30	0.22	0.61	0.56	0.68	0.56	0.89
Mn	0.01	0.01	0.01	0.02	0.01	0.00	0.00	0.02	0.02	0.02	0.02	0.03
Ca	0.90	0.83	0.64	0.79	0.88	0.85	0.90	0.91	0.89	0.90	0.75	0.06
Na	0.05	0.04	0.03	0.04	0.03	0.04	0.04	0.03	0.03	0.07	0.02	0.00
Total	4.00	4.00	4.00	4.00	4.00	4.00	4.00	4.00	4.00	4.00	4.00	4.00
X_{Wo}	0.462	0.420	0.314	0.393	0.449	0.429	0.461	0.459	0.454	0.481	0.374	0.030
X_{En}	0.406	0.430	0.508	0.301	0.348	0.403	0.419	0.212	0.249	0.141	0.333	0.511
X_{Fs}	0.133	0.151	0.177	0.306	0.203	0.168	0.120	0.330	0.296	0.379	0.292	0.460

Not determined (–).

small compositional range within the sample suite ($En_{41}Fs_{16}Wo_{42}$ to $En_{34}Fs_{22}Wo_{44}$) (Fig. 4c). Augite rims around olivine are strongly zoned showing an increase in Fs component with increasing distance from the olivine grain ($En_{42}Fs_{11}Wo_{47}$ to $En_{31}Fs_{22}Wo_{47}$). Augites of the syenitic samples span a large range in composition ($En_{40}Fs_{19}Wo_{41}$ to $En_8Fs_{47}Wo_{45}$), partly overlapping with augites of the gabbroic samples. Due to strong chemical zoning, the compositional variation within one single grain may reach as much as 20 mol% (Fig. 5). Among the investigated syenitic samples, three different zoning patterns can be distinguished: In most cases, $X_{Fe} = Fe^{2+}/(Fe^{2+} + Mg)$, Fe^{3+}, Na and Si increase, and Ti and Al(4) decrease more or less continuously from core to rim, whereas the wollastonite component is almost constant (Fig. 5a). Some samples have Mg-rich cores, and display a stepwise increase of X_{Fe} from core to rim (Fig. 5b). In other samples, partly resorbed inner cores of clinopyroxene are Fe- and Si-rich, followed by a homogeneous but significantly Fe-depleted outer rim with a normal increase of X_{Fe} towards the rim. Interestingly, Na, Al(4), $Fe^{3+}$and Ti contents in these crystals is more or less constant throughout the whole profile (Fig. 5c).

Clinopyroxene in the larvikite is relatively Ca-poor with a compositional range between $En_{44}Fs_{17}Wo_{39}$ and $En_{29}Fs_{32}Wo_{39}$ (Fig. 4d).

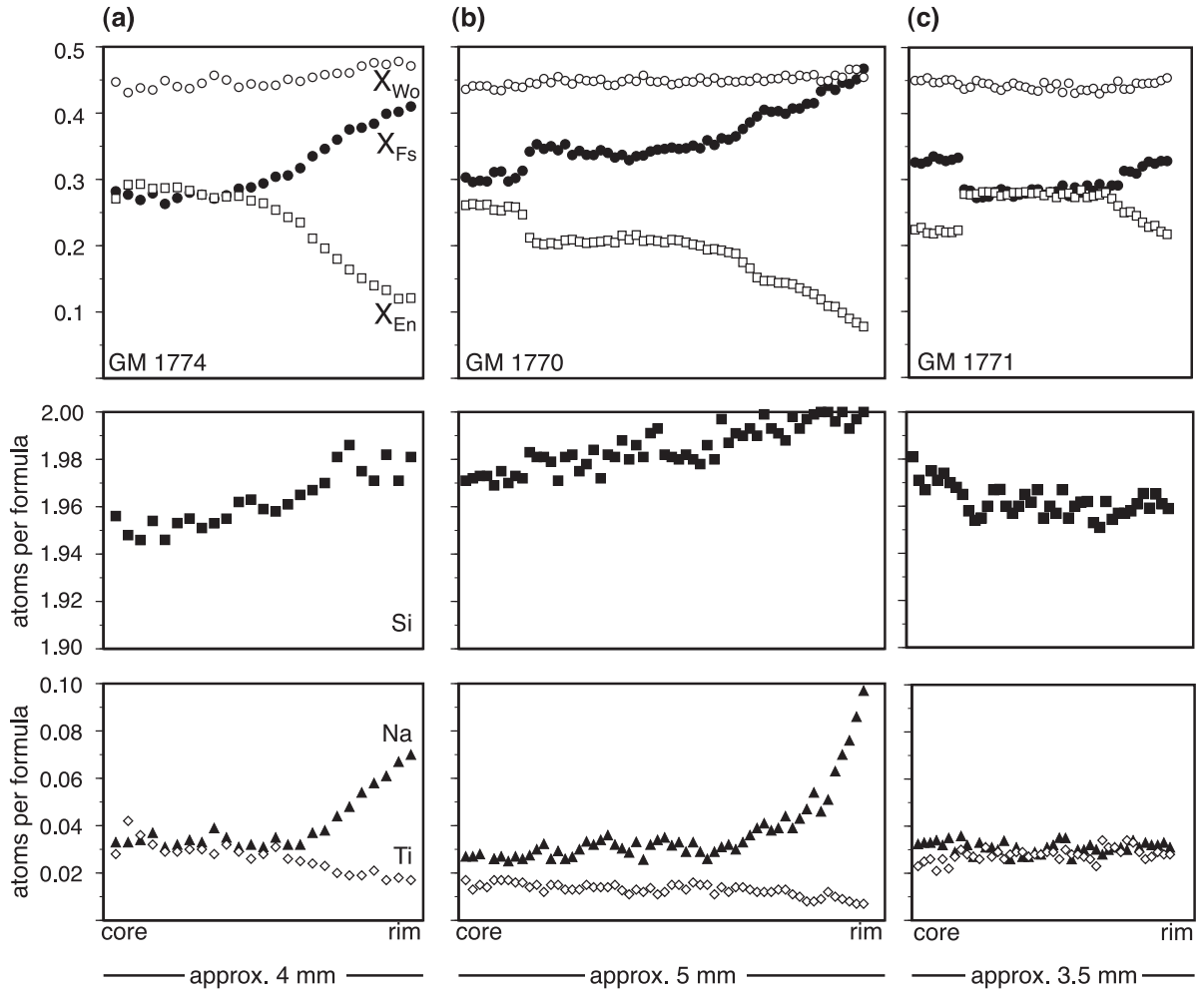

Fig. 5. Zoning profiles in clinopyroxenes of Giant Dike 3.

4.2.4. Orthopyroxene

Orthopyroxene is only present in the larvikite where it occurs as small rims around olivine (Fig. 2c). It is chemically unzoned with a composition of $En_{52}Fs_{47}Wo_1$ to $En_{50}Fs_{49}Wo_1$.

4.2.5. Fe–Ti oxides

Typical compositions of exsolved and reintegrated Fe–Ti oxides are presented in Table 5. In most samples, primary titanomagnetite is oxy-exsolved to ilmenite and magnetite (Fig. 6a–d).

The olivine–gabbro contains a single oxy-exsolved titanomagnetite with very Ti-rich compositions ($Usp_{94-95}Sp_{3-4}Mag_2$), which is characterized by a very fine trellis-type exsolution texture (terminology after Buddington and Lindsley, 1964; Fig. 6a).

In BFDs 1 and 3, more coarsely trellis-type oxy-exsolved titanomagnetite is common, but there are also Fe–Ti oxide grains where it is difficult to decide whether they represent a single oxy-exsolved grain with a granule exsolution texture or two coexisting oxides. In those cases, oxides with trellis-type exsolution were preferentially used for reintegration resulting in compositions between $Usp_{89}Sp_3Mag_7$ and $Usp_{65}Sp_4Mag_{31}$ (Fig. 6b). In BFD 4, a two-oxide assemblage comprises $Usp_{71-58}Sp_{9-5}Mag_{24-37}$ coexisting with $Ilm_{98-96}Hem_{2-4}$.

Table 5
Representative analyses of unexsolved magnetite and ilmenite, exsolved magnetite and ilmenite and calculated bulk compositions

Dike	BFD 4		Larvikite		BFD 1			GD 3, gabbro			GD 3, gabbro		
Sample	GD 39		GM 1684		GM 1680			GM 1762			GM 1762		
Texture	Mag unexs.	Ilm unexs.	Mag unexs.	Ilm unexs.	Mag exs.	Ilm exs.	Bulk calc.	Mag exs.	Ilm exs.	Bulk calc.	Mag exs.	Ilm exs.	Bulk calc.
wt.%													
SiO_2	0.02	0.00	0.05	0.00	0.00	0.00	0.00	0.00	0.00	0.00	0.03	0.02	0.02
TiO_2	25.07	51.98	7.36	50.15	15.42	53.21	26.44	15.44	51.80	32.95	11.34	51.77	25.12
Al_2O_3	2.52	0.12	1.35	0.02	1.05	0.01	0.74	2.20	0.01	1.15	2.35	0.02	1.56
Cr_2O_3	0.17	0.04	0.18	0.02	0.11	0.06	0.10	0.02	0.00	0.01	0.00	0.00	0.00
ZnO	0.03	0.01	–	–	0.09	0.04	0.07	0.10	0.00	0.05	0.19	0.00	0.12
FeO	68.22	44.47	84.98	47.19	78.81	45.07	68.97	77.56	46.51	62.61	80.77	46.49	69.09
MnO	0.90	0.68	0.45	1.96	0.74	2.28	1.19	0.43	1.39	0.89	0.36	1.42	0.72
MgO	1.05	2.30	0.00	0.00	0.00	0.00	0.00	0.00	0.00	0.00	0.00	0.00	0.00
CaO	0.05	0.03	–	–	0.00	0.00	0.00	0.03	0.03	0.03	0.18	0.04	0.14
Total	98.02	99.63	94.37	99.33	96.22	100.67	97.51	95.77	99.74	97.65	95.22	99.76	96.63
Formulae based on three (two) cations and four (three) oxygens for mag (ilm)													
Si	0.00	0.00	0.00	0.00	0.00	0.00	0.00	0.00	0.00	0.00	0.00	0.00	0.00
Al	0.11	0.00	0.06	0.00	0.05	0.00	0.03	0.10	0.00	0.05	0.10	0.00	0.07
Ti	0.69	0.97	0.21	0.95	0.44	1.00	0.75	0.44	0.99	0.94	0.32	0.98	0.71
Cr	0.01	0.00	0.01	0.00	0.00	0.00	0.00	0.00	0.00	0.00	0.00	0.00	0.00
Fe^{3+}	0.49	0.05	1.51	0.09	1.08	0.00	0.46	1.03	0.03	0.07	1.25	0.03	0.50
Mg	0.06	0.09	0.00	0.00	0.00	0.00	0.00	0.00	0.00	0.00	0.00	0.00	0.00
Fe^{2+}	1.61	0.87	1.20	0.91	1.41	0.95	1.71	1.42	0.95	1.91	1.30	0.95	1.68
Mn	0.03	0.01	0.01	0.04	0.02	0.05	0.04	0.01	0.03	0.03	0.01	0.03	0.02
Zn	0.00	0.00	–	–	0.00	0.00	0.00	0.00	0.00	0.00	0.01	0.00	0.00
Ca	0.00	0.00	–	–	0.00	0.00	0.00	0.00	0.00	0.00	0.01	0.00	0.01
Sum	3.00	2.00	3.00	2.00	3.00	2.00	3.00	3.00	2.00	3.00	3.00	2.00	3.00
mol%													
Usp/Ilm	0.70	0.97	0.21	0.96	0.44	1.00	0.75	0.44	0.99	0.94	0.32	0.99	0.71
Mag/Hem	0.25	0.03	0.76	0.04	0.54	0.00	0.23	0.51	0.01	0.04	0.63	0.01	0.25
Sp	0.05		0.03		0.02		0.02	0.05		0.03	0.05		0.03
For QUILF													
Nti/Nhem	0.697	0.026	0.211	0.043	0.438	0.000	0.751	0.439	0.014	0.938	0.323	0.015	0.716
NMg/NGk	0.056	0.085	0.000	0.000	0.000	0.000	0.000	0.000	0.000	0.000	0.000	0.000	0.000
NMn/NPy	0.28	0.014	0.015	0.042	0.024	0.049	0.038	0.014	0.030	0.029	0.012	0.030	0.023

Unexsolved (unexs.), exsolved (exs.), calculated (calc.); NTi, NMn, NMg and NHem, NPy, NGk are QUILF-specific parameters for magnetite and ilmenite, respectively (see Andersen et al., 1993); not determined (–).

Gabbroic samples of Giant Dike 3 contain a two-oxide assemblage of titanomagnetite ($Usp_{94-70}Sp_3Mag_{4-27}$) coexisting with ilmenite ($Ilm_{99-96}Hem_{1-4}$). The intermediate sample of Giant Dike 1 contains a single exsolved titanomagnetite of the composition $Usp_{93-83}Sp_3Mag_{5-14}$. In syenitic samples, primary titanomagnetite compositions could not be recalculated because both exsolved ilmenite and magnetite were strongly altered to titanite/Fe-rich chlorite and chlorite/Fe-hydroxides, respectively (Fig. 6c). However, relics of exsolved magnetite ($Usp_{19-8}Sp_{5-3}Mag_{78-87}$) still have elevated Ti contents indicating an Usp-rich primary composition of titanomagnetite.

The larvikite contains a two-oxide assemblage, but textural evidence suggests that ilmenite was overgrown by later magnetite (Fig. 6d). Both have a relatively constant composition of $Ilm_{97-94}Hem_{6-3}$ and $Usp_{27-21}Sp_{4-3}Mag_{70-76}$, respectively. The hornblende–syenite contains only primary ilmenite of the composition $Ilm_{98-89}Hem_{2-11}$.

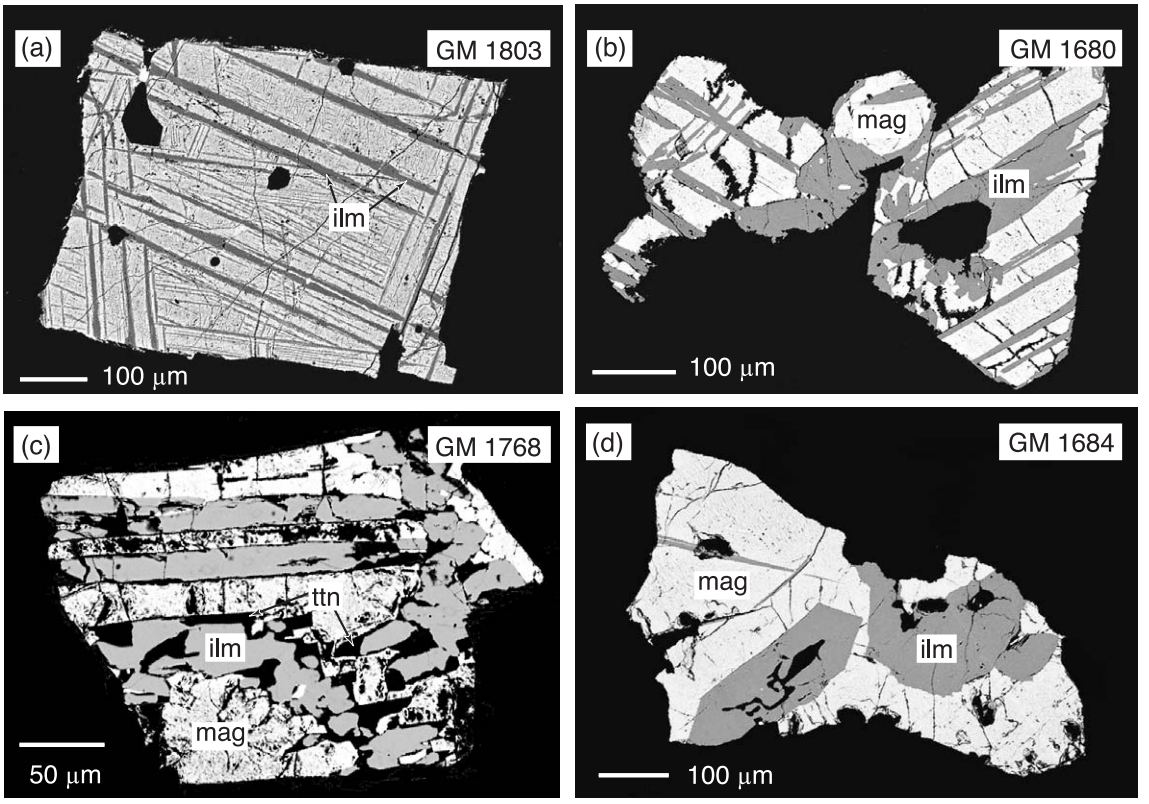

Fig. 6. BSE images of Fe–Ti oxides in Isortoq dike rocks. (a) Fine trellis-type exsolution in the olivine–gabbro, (b) coarse trellis-type exsolution in BFD 1, (c) alteration of Fe–Ti oxides to titanite in the syenitic facies of Giant Dike 3, (d) ilmenite overgrown by magnetite in the larvikite.

4.3. Calculation of intensive crystallization parameters

Intensive crystallization parameters were calculated because estimates of liquidus and solidus temperatures of the dike magmas are essential for energy constrained AFC modeling (Spera and Bohrson, 2001) and calculated values of silica activity and oxygen fugacity may provide important constraints on the evolution of the dike magmas. For all calculations, pressure was fixed at 1 kbar, assuming that crystallization of the dikes took place at approximately the same depth as of the Ilímaussaq complex further south in the Gardar Province for which a crystallization pressure of ~ 1 kbar was derived from fluid inclusion data (Konnerup-Madsen and Rose-Hansen, 1984).

Liquidus temperatures were calculated for some olivine-bearing samples, which are considered to be close to liquid compositions (GM 1803, GM 1735, GM 1805 and GD 39) after Sugawara (2000) based on the MgO content in olivine-saturated liquids. They range between 1145 and 1120 °C with an error in calculated temperatures of ± 30 °C.

Feldspar geothermometry using solvus isotherms after Elkins and Grove (1990) indicates minimum crystallization temperatures of ~ 700 °C for BFD 1 as an example for the gabbroic BFDs and the olivine–gabbro (Fig. 3a). Plagioclase–alkali feldspar pairs in the gabbroic samples of Giant Dike 3 and in the larvikite are not in equilibrium. As shown in Fig. 2d, plagioclase has reacted with the liquid to produce alkali feldspar. Ternary feldspar compositions in gabbroic and syenitic samples of Giant Dike 3 point to minimum temperatures of 950–1020 °C (Fig. 3b). A zoning profile through an alkali feldspar in the larvikite show continuously decreasing minimum temper-

atures from >1000° in the core to about 700 °C in the outermost rim (Fig. 3c).

Solidus temperatures, silica activity and oxygen fugacity were calculated from olivine–pyroxene–Fe–Ti oxide equilibria using the QUILF program of Andersen et al. (1993). The theoretical background for these calculations was given by Frost and Lindsley (1992) and Lindsley and Frost (1992). Temperature and silica activity were calculated based on Fe, Mg and Ca exchange between olivine and clinopyroxene using a range of mineral compositions. Calculated silica activities are based on a reference state of pure SiO_2 at P and T. The oxygen fugacity was calculated from equilibria among Fe–Mg silicates and Fe–Ti oxides using the full range of measured and reintegrated Fe–Ti oxide compositions. Details of the use of QUILF can be found in Marks and Markl (2001).

Calculated equilibrium temperatures for the olivine–gabbro, the BFDs, and for gabbroic samples of the Giant Dike 3 range between 930 and 850 °C. Calculated silica activities are 0.60 in the olivine–gabbro, 0.67–0.83 in the quartz-free BFDs, and 0.53–0.68 in the Giant Dike profile. The clinopyroxene rims around olivine in two gabbroic samples of Giant Dike 3 indicate an increase in silica activity. In the syenitic samples, olivine has disappeared due to a further increase in silica activity during progressive fractionation. Unreasonably low calculated temperatures (< 650 °C) for the larvikite indicate that very rare olivine is not in chemical equilibrium with clinopyroxene. Using a calculated olivine equilibrium composition of Fo_{56} and a range of early ilmenite compositions, the resulting silica activity is 0.83, which is within the upper range obtained for the gabbroic samples. The orthopyroxene rim around olivine indicates increasing silica activities during later stages. This is in accordance with petrography, as interstitial quartz is present and thus, final solidification of the larvikite took place at $a_{SiO2} = 1$.

Generally, the calculated oxygen fugacity increases with increasing silica activity from about 3 log units below the fayalite–magnetite–quartz (FMQ) buffer in the olivine–gabbro to values slightly above the FMQ buffer in some BFD samples, with the gabbroic samples of Giant Dike 3 in between (Fig. 7). The absence of primary ilmenite the syenitic samples of Giant Dike 3 indicates that oxygen fugacity in the syenitic samples was higher than in gabbroic samples of Giant Dike 3 (Toplis and Carroll, 1995). For the larvikite, oxygen

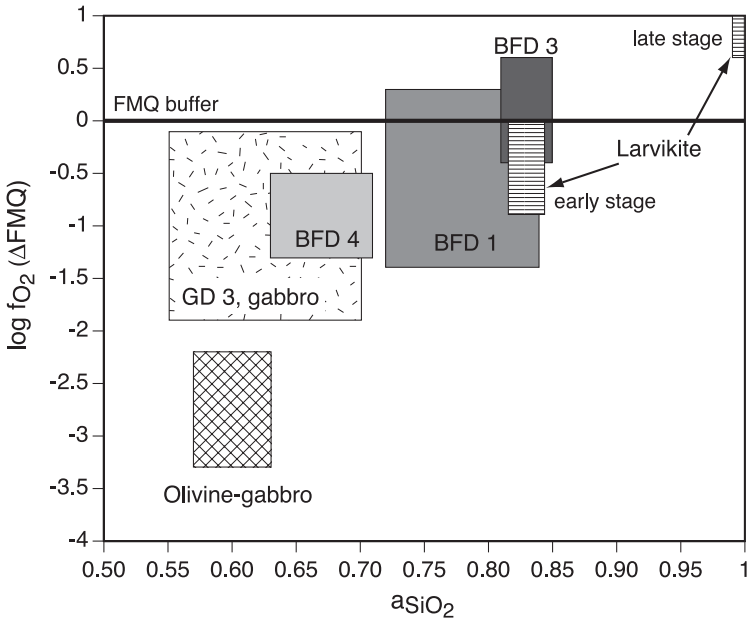

Fig. 7. Oxygen fugacity vs. silica activity in Isortoq dike rocks, calculated with QUILF (Andersen et al., 1993). Please note that BFD 2 and the hornblende–syenite were omitted for QUILF calculations due of the lack of suitable mineral parageneses, but they should plot at $a_{SiO2} = 1$.

fugacity was calculated only with ilmenite, as textural relationships (Fig. 6d) indicate that magnetite grew later. It varies between 0 and 0.9 log units below FMQ at $T = 853$ °C. Oxygen fugacity calculated with the assemblage Fe-rich clinopyroxene + titanomagnetite ± orthopyroxene at temperatures fixed between 850 and 700 °C to simulate gradual cooling during later stages indicates more oxidizing conditions of 0.6–1.0 log units above the FMQ buffer.

4.4. REE data of clinopyroxenes

REE concentrations of average clinopyroxenes from the Isortoq dike rocks are presented in Table 6 and typical chondrite-normalized REE patterns of individual and average analyses are shown in Fig. 8. Because closed-system fractionation can result in considerable fractionation of the REE (Bernstein et al., 1998), rims of clinopyroxenes were avoided for analyses. Clinopyroxenes of all dikes are enriched in REE relative to chondritic values. The patterns generally show an increase in normalized REE contents from La to Nd, followed by a gradual decrease from Sm to Lu. Significant Eu anomalies are lacking in the BFDs, but there is a small negative Eu anomaly in the olivine–gabbro (Eu/Eu* = 0.70). In the Giant Dikes, a negative Eu anomaly is increasing from Eu/Eu* = 0.81 in the relatively primitive gabbroic facies, via 0.65 in an intermediate syenogabbro towards 0.41 in the more fractionated syenitic rocks. A similar evolution can be seen in the larvikite, where the extent of the negative Eu anomaly is positively correlated with the degree of REE enrichment, i.e., fractionation. Taking La_N/Yb_N as a measure for REE fractionation, two observations may be of importance. First, the olivine–gabbro has a less fractionated clinopyroxene REE pattern than the BFDs, but it has a more pronounced negative Eu anomaly. Second, La_N/Yb_N in the low-Ca clinopyroxene inclusions is considerably lower than in any of the dike matrix clinopyroxenes. Clinopyroxenes from

Table 6
Average Laser-ICP-MS analyses of REEs in clinopyroxene from Isortoq dike rocks

Dike	Olivine–gabbro	BFD 1	BFD 1	BFD 1	BFD 1	BFD 1	BFD 1	BFD 1 anorthosite xenolith	BFD 3	GD 1 syenogabbro	GD 3 gabbro	GD 3 syenite	Larvikite
Sample	GM 1803	GM 1680	GM 1729	GM 1735	GM 1681 matrix	GM 1681 high-Ca inclusions	GM 1681 low-Ca inclusions	GM 1682	GM 1805	GM 1712	GM 1760	GM 1772	GM 1684
No. of cpx analyzed	$n=7$	$n=3$	$n=3$	$n=6$	$n=2$	$n=4$	$n=3$	$n=4$	$n=4$	$n=3$	$n=11$	$n=11$	$n=4$
REE concentrations in ppm													
La	7.58	5.60	6.43	8.02	16.53	10.28	2.59	4.18	10.90	10.25	11.55	18.46	13.38
Ce	32.65	27.72	27.30	32.46	64.06	37.77	12.30	16.84	39.26	38.52	42.36	59.64	52.13
Pr	6.28	4.70	5.30	6.07	12.93	6.99	2.93	3.44	7.58	7.78	8.02	11.14	9.50
Nd	34.60	27.53	29.36	38.96	74.00	40.49	18.40	20.40	45.97	43.07	45.54	59.32	56.88
Sm	10.93	8.29	8.20	11.67	18.27	11.63	6.57	7.04	13.39	13.44	13.44	16.15	14.89
Eu	2.60	2.73	2.75	3.54	4.70	3.39	2.16	2.46	3.90	2.72	3.43	1.85	3.41
Gd	11.61	8.27	7.76	12.06	12.40	11.03	8.11	7.73	12.50	13.35	13.35	14.01	12.70
Tb	1.83	1.30	1.25	1.86	1.76	1.96	1.29	1.08	2.17	2.50	2.12	2.31	1.92
Dy	10.81	7.56	7.22	10.87	11.09	11.07	7.95	5.83	11.94	13.72	12.02	13.17	10.63
Ho	2.05	1.42	1.47	2.12	2.22	2.22	1.63	1.19	2.17	2.78	2.46	2.71	2.01
Er	5.67	3.39	3.54	5.17	6.26	5.85	4.19	2.75	5.55	7.09	6.18	7.19	5.48
Tm	0.78	0.47	0.52	0.74	1.17	0.88	0.66	0.55	0.80	0.94	0.92	1.10	0.77
Yb	5.75	3.43	3.25	5.03	9.31	5.84	4.04	2.78	5.72	7.03	6.18	8.99	5.83
Lu	0.86	0.45	0.49	0.72	1.82	0.92	0.74	0.49	0.76	1.03	0.96	1.80	0.84
LaN/YbN	0.89	1.10	1.33	1.07	1.20	1.19	0.43	1.01	1.28	0.98	1.26	1.38	1.55
Eu/Eu*	0.70	1.00	1.07	0.92	0.98	0.92	0.91	1.02	0.93	0.65	0.81	0.41	0.89
Eu/Eu*max	0.74	1.04	1.13	0.98	1.06	0.93	1.13	1.08	1.16	0.80	0.96	0.78	1.20

$Eu/Eu^* = EuN/(SmN \times GdN)^{0.5}$; Eu/Eu^*_{max} is the maximum value of Eu/Eu* in an individual clinopyroxene of the respective sample.

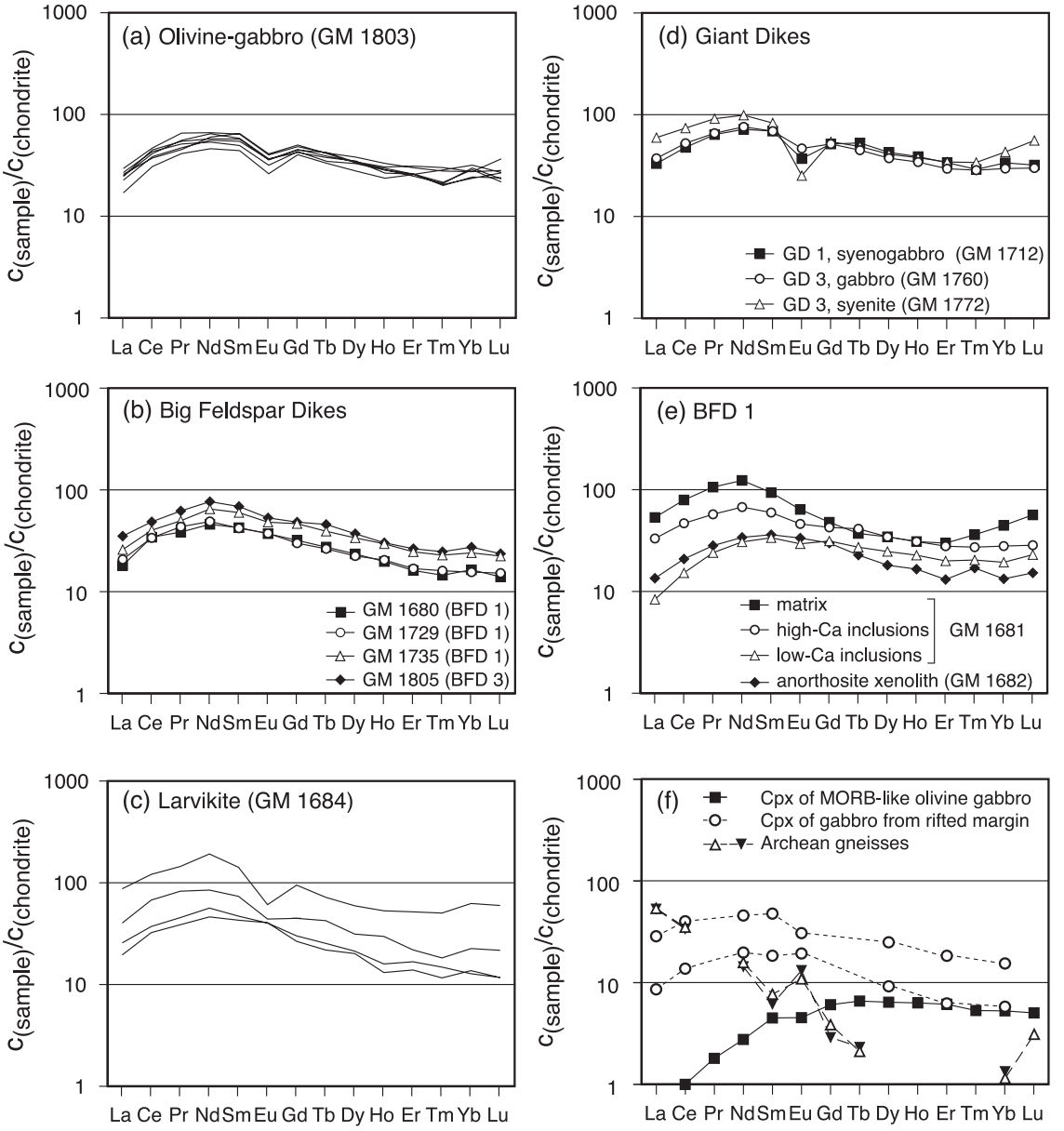

Fig. 8. REE patterns of clinopyroxenes from Isortoq dike rocks, normalized to chondritic values from Boynton (1984). Individual clinopyroxene analyses are shown in Panels a and c; all other diagrams show averaged values. REE patterns of clinopyroxenes from MORB-like olivine–gabbro (Benoit et al., 1996) and gabbro from a rifted continental margin (Bernstein et al., 1998) together with whole-rock REE data from two Archean gneisses (Compton, 1978) are shown for comparison.

all dike rocks have REE patterns similar to gabbros from the rifted East Greenland margin (Bernstein et al., 1998), but distinct from gabbros derived from a MORB-like source.

4.5. Whole-rock geochemistry

XRF whole-rock data of the dike rocks are presented in Table 7 and the compositional variation with

Table 7
XRF whole-rock analyses of Isortoq dike rocks

Dike	Olivine–gabbro	BFD 1	BFD 1 anorthosite xenolith	BFD 2	BFD 3	BFD 4	GD 1 syeno-gabbro	GD 3 gabbro	GD 3 syenite	GD 3 syenite	Larvikite	Hbl.–syenite
Sample	GM 1803	GM 1735	GM 1682	GM 1750	GM 1805	GD 39	GM 1712	GM 1760	GM 1772	GM 1778	GM 1684	GD 38
Major elements (wt.%)												
SiO_2	44.57	46.46	51.86	53.05	49.88	46.73	47.83	41.69	55.17	55.93	56.34	53.91
TiO_2	2.95	2.25	1.76	1.83	1.93	2.67	2.12	4.19	1.55	1.55	1.28	0.97
Al_2O_3	16.79	16.62	19.32	17.56	15.83	16.03	18.54	14.09	15.41	15.37	16.87	16.62
Fe_2O_3	15.90	14.11	8.82	9.81	12.92	14.92	12.30	17.03	10.50	10.91	8.50	8.57
MnO	0.19	0.17	0.12	0.15	0.17	0.19	0.16	0.22	0.20	0.20	0.14	0.13
MgO	5.08	5.54	2.12	2.17	4.34	5.72	2.59	4.71	1.10	0.99	2.35	4.06
CaO	7.68	7.40	7.62	6.12	6.72	7.77	7.26	8.22	4.16	3.67	4.82	6.11
Na_2O	3.69	3.68	4.58	4.40	4.41	3.74	4.46	3.69	5.18	5.86	4.75	4.01
K_2O	1.12	1.25	1.63	2.78	1.48	1.18	1.89	1.79	4.03	3.34	3.26	2.48
P_2O_5	0.48	0.47	0.45	0.68	0.40	0.56	0.47	2.48	0.44	0.40	0.33	0.43
LOI	0.67	0.64	0.88	0.56	0.66	−0.43	2.09	0.84	0.64	0.86	0.67	1.91
Total	99.12	98.59	99.16	99.11	98.74	99.08	99.71	98.95	98.38	99.08	99.31	99.20
Mg#[a]	43.2	48.3	36.4	34.5	44.4	47.7	33.4	39.7	19.9	17.7	39.7	53.0
Trace elements (ppm)												
Sc	17	21	15	18	20	20	14	17	13	10	16	20
V	173	193	86	83	174	162	96	107	6	3	78	155
Cr	36	54	2	4	44	70	n.d.	n.d.	n.d.	n.d.	29	45
Co	62	78	18	22	60	84	40	47	6	7	55	60
Ni	53	87	11	14	60	71	29	n.d.	3	n.d.	34	33
Cu	37	61	10	12	67	47	26	27	n.d.	n.d.	46	46
Zn	92	105	76	85	109	104	86	96	130	124	101	102
Ga	18	20	20	19	21	19	21	15	19	22	23	19
Rb	19	17	15	35	25	14	33	18	32	36	33	60
Sr	411	629	753	563	510	454	558	421	417	265	535	817
Y	30	24	25	32	31	34	42	39	45	51	27	27
Zr	172	140	137	215	221	171	245	150	271	367	245	163
Nb	12	14	11	14	14	12	18	12	22	25	16	14
Ba	463	750	1022	1740	936	649	899	718	2981	2131	2513	972
Pb	4	5	7	9	7	4	15	7	8	11	15	8
La	–	–	24	41	–	16	–	–	38	42	–	35
Ce	–	–	62	95	–	65	–	–	96	101	–	93
Pr	–	–	4	8	–	6	–	–	9	7	–	7
Nd	–	–	31	52	–	32	–	–	51	49	–	44
Sm	–	–	4	9	–	10	–	–	5	8	–	8
Characteristic normative minerals[b]	*ne + ol*	*ne + ol*	*hy + ol*	*hy + ol*	*hy + ol*	*ne + ol*	*ne + ol*	*ne + ol*	*ne + ol*	*hy + ol*	*q + hy*	*q + hy*

Not detected (n.d.); not determined (–).
[a] $Mg\# = 100[Mg/(Mg + Fe^{2+})]$ with $Fe_2O_3/FeO = 0.2$.
[b] Calculation of normative mineral composition according to the CIPW norm.

respect to Mg# as fractionation index is shown in Fig. 9. Mg-numbers [$Mg\# = 100\ Mg/(Mg + Fe^{2+})$ atomic] were calculated using a Fe_2O_3/FeO ratio of 0.2 (Middlemost, 1989) for all rock types as the Ti-rich oxides from all samples indicate relatively reducing conditions even in more fractionated rocks. Mg# between 53 and 18 indicate that the samples do not represent primary melts. SiO_2 contents appear to be relatively scattered, but there is a distinct negative correlation within the BFD and the Giant Dike samples. The

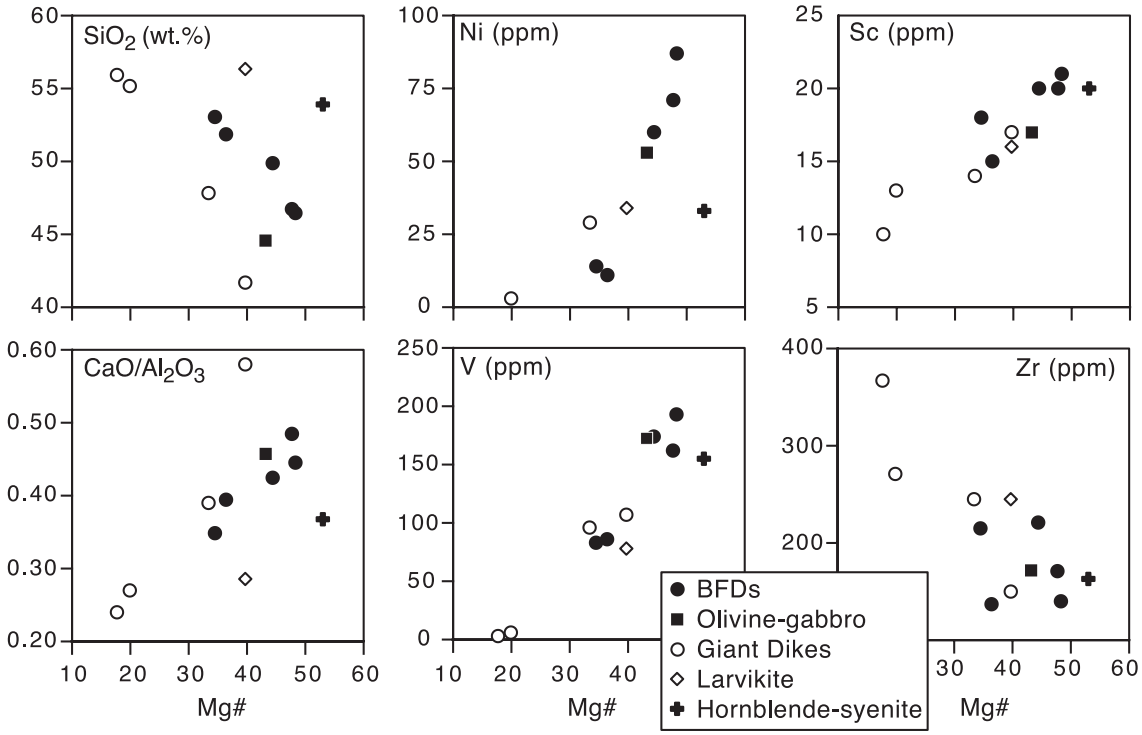

Fig. 9. Whole-rock variation diagrams for Isortoq dike rocks with Mg# = Mg/(Mg + Fe^{2+}) as fractionation index.

positive correlation of CaO/Al_2O_3 with Mg# suggests fractionation of clinopyroxene (e.g., Cox et al., 1979; Class et al., 1994). The larvikite and the hornblende–syenite are characterized by higher SiO_2 and lower CaO/Al_2O_3 values. The high P_2O_5 and TiO_2 concentrations in Giant Dike sample GM 1760 (Table 7), combined with the high modal apatite content, indicates that this sample was affected by apatite and possibly Fe–Ti oxide accumulation.

Maximum Ni and Cr contents of 87 and 70 ppm, respectively, confirm that the dikes crystallized from relatively fractionated melts. Other trace elements compatible in mafic systems (e.g., V and Sc) also have relatively low concentrations. Ni and Sc are positively correlated with Mg# suggesting fractionation of olivine and clinopyroxene. A positive correlation of Cr contents with Mg# in the BFDs is a further indication that olivine and/or clinopyroxene fractionation operated in the magmas (not shown). V, which is highly compatible in magnetite and slightly compatible in clinopyroxene, is also decreasing with decreasing Mg#, indicating fractionation of Fe–Ti oxides. Incompatible trace elements like Zr show a weak negative correlation with Mg# for the Giant Dike samples consistent with increasing degrees of differentiation, but the BFD samples are rather scattered.

Normative mineral compositions were calculated following the CIPW scheme (Cross et al., 1903; Cox et al., 1979) and characteristic normative minerals are listed in Table 7. The olivine–gabbro and the BFDs are variably *ne*- and *hy*-normative. In the Giant Dikes, normative compositions change from *ne*-normative in the gabbros to *hy*-normative in the syenites. The *qz*-normative larvikite and hornblende–syenite both contain modal quartz indicating that the normative compositions accurately reflect the modal mineralogy. However, BFD 2 (GM 1750) and the anorthosite xenolith (GM 1682) have late interstitial quartz, but they are quartz-free in the norm calculation. This might be due to the fact that small errors in the assumed Fe^{2+}/Fe^{3+} ratio can lead to variable normative mineral compositions. In summary, the calculations of the normative mineral compositions demonstrate that the least fractionated rocks are silica

undersaturated. The most fractionated rocks, represented by the syenites of the Giant Dikes, evolved towards *hy*-normative compositions. *Qz*-normative compositions of the larvikite and the hornblende–syenite are not coupled to a low Mg#.

Primitive mantle-normalized incompatible trace element diagrams for selected samples are shown in Fig. 10. The patterns are characterized by a general enrichment relative to primitive mantle values and distinct Ba peaks and Nb troughs. The Ba peak in the hornblende–syenite is considerably smaller than in all other dikes. Small negative P and Ti anomalies are present in the two syenitic samples, and the GD 3 syenite has also a negative Sr anomaly. The two BFD samples have fairly smooth patterns from La to Y with a small positive Sr anomaly in the anorthosite xenolith and a small negative one in BFD 4.

4.6. Sr and Nd isotopic compositions

Sr and Nd isotopic compositions of mineral separates from the dikes and of whole-rocks from the Julianehåb batholith are presented in Table 8. Using the Sm–Nd system on mineral separates of clinopyroxene and plagioclase and whole-rock powder (Table 8, Fig. 11), we dated sample GM 1735 from BFD 1. The age of 1190 ± 44 Ma agrees well with that of the Bangs Havn Giant Dike (1185 ± 22 Ma; Engell and Pedersen, 1974) which is thought to be of the same age. The three clinopyroxene separates from Giant Dike 3 give an age of 1187 ± 87 Ma, consistent with the BFD 1 and the Bangs Havn Giant Dike ages. These ages also agree with field evidence, as the Isortoq swarm is cut by the Nunarssuit syenite, which was dated by the U/Pb method at 1171 ± 5 Ma (Finch et al., 2001), and postdates the older "Brown dikes" dated at 1280 ± 5 Ma (Upton et al., 2003).

$^{87}Sr/^{86}Sr$ initial ratios of the dikes at 1.19 Ga range from 0.70289 to 0.70432 and $\varepsilon_{Nd}(i)$ values from +0.3 to −10.7 (Table 8). On the Sr–Nd isotope diagram, the data define a relatively steep trend (Fig. 12) with initial $^{87}Sr/^{86}Sr$ ratios of the isotopically more primitive samples similar to Bulk Silicate Earth (BSE). The olivine–gabbro and the Giant Dikes have $\varepsilon_{Nd}(i)$ values clustering around 0 to −2, whereas the BFDs show a clear tendency towards more negative $\varepsilon_{Nd}(i)$ values. None of the samples has $\varepsilon_{Nd}(i)$ values close to those of the depleted MORB mantle (DMM) reservoir, estimated to be between $\varepsilon_{Nd}(i)$=+5.3 (calculated after DePaolo, 1981) and $\varepsilon_{Nd}(i)$=+7.4 (calculated after Goldstein et al., 1984).

In comparison with other Sr–Nd data from the Gardar Province, the Isortoq dikes extend the range of $\varepsilon_{Nd}(i)$ towards significantly more negative values than previously reported. The isotopically more primitive dikes overlap with data from the Eriksfjord Formation

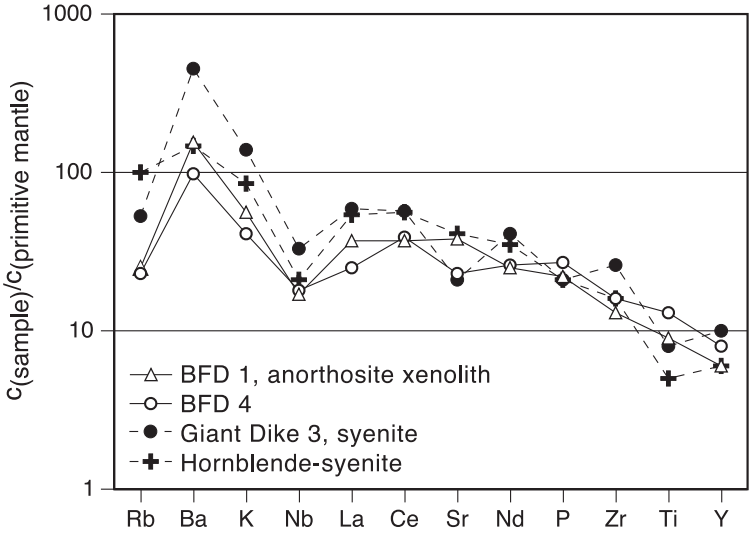

Fig. 10. Multielement plot of selected Isortoq samples normalized to primitive mantle values from McDonough and Sun (1995).

Table 8
Sr, Nd and O isotopic composition of Isortoq dike rocks and adjacent Ketilidian basement rocks

Rock type	Sample	Material	Sr (ppm)	Rb (ppm)	$^{87}Rb/^{86}Sr$	$^{87}Sr/^{86}Sr$	$^{87}Sr/^{86}Sr(i)$	Sm (ppm)	Nd (ppm)	$^{147}Sm/^{144}Nd$	$^{143}Nd/^{144}Nd$	$\varepsilon_{Nd}(i)\delta^{18}O$	(V-SMOW)
Isortoq dikes													
BFD 1	GM 1682	cpx	41.60	0.800	0.0556	0.704454 ± 10	0.70351	13.56	47.42	0.1728	0.512165 ± 09	− 5.6	5.73
Anorthosite xenolith													
Larvikite	GM 1684	cpx	52.31	1.087	0.0601	0.705016 ± 10	0.70399	14.35	53.20	0.1631	0.511830 ± 10	− 10.7	6.20
GD 1, gabbro	GM 1712	cpx	56.42	0.361	0.0185	0.703728 ± 10	0.70341	19.94	66.67	0.1808	0.512484 ± 10	− 0.6	5.30
BFD 1	GM 1735	cpx	61.40	3.085	0.1453	0.705773 ± 10	0.70330	16.16	58.51	0.1670	0.512223 ± 10	− 3.6	5.72 ± 0.07
BFD 1	GM 1735	whole-rock						5.64	26.06	0.1308	0.511922 ± 10	− 3.9	
BFD 1	GM 1735	plagioclase						2.14	11.74	0.1100	0.511780 ± 10	− 3.5	6.61 ± 0.08
BFD 2	GM 1750	cpx	51.41	7.337	0.4130	0.709994 ± 10	0.70296	19.03	74.61	0.1542	0.511902 ± 09	− 7.9	5.93
GD 3, gabbro	GM 1760	cpx	44.96	0.739	0.0475	0.704151 ± 10	0.70334	14.80	51.87	0.1725	0.512357 ± 10	− 1.8	5.62
GD 3, syenite	GM 1772	cpx	44.92	0.973	0.0627	0.704572 ± 10	0.70350	22.06	91.46	0.1458	0.512146 ± 14	− 1.8	5.41
GD 3, syenite	GM 1778	cpx	32.87	1.128	0.0993	0.704920 ± 09	0.70323	20.03	82.24	0.1472	0.512163 ± 10	− 1.7	
Olivine–gabbro	GM 1803	cpx	49.32	1.177	0.0690	0.704069 ± 10	0.70289	21.09	73.19	0.1742	0.512475 ± 10	0.3	5.54
BFD 3	GM 1805	cpx	58.67	1.399	0.0690	0.704794 ± 09	0.70362	13.45	47.63	0.1706	0.512079 ± 10	− 6.9	5.59
Brown Dike (BD_0)	GD 37	cpx	44.61	0.218	0.0141	0.703721 ± 09	0.70346	5.79	16.65	0.2103	0.512619 ± 10	− 2.6	
Hornblende–syenite	GD 38	amph	101.10	5.863	0.1677	0.707176 ± 10	0.70432	18.99	83.46	0.1376	0.511959 ± 10	− 4.2	5.21
BFD 4	GD 39	cpx	67.57	0.391	0.0167	0.703431 ± 09	0.70315	12.62	41.66	0.1831	0.512479 ± 10	− 1.0	
Ketilidian basement													
Granitoid	BT 03	whole-rock	70.58	186.9	7.8080	0.901275 ± 09	0.76821	8.25	54.67	0.0913	0.511341 ± 10	− 9.3	8.2
Granitoid	BT 05	whole-rock	946.4	31.96	0.0977	0.704834 ± 16	0.70317	1.94	10.16	0.1154	0.511785 ± 10	− 4.3	7.2
Granitoid	BT 06	whole-rock	422.1	109.2	0.7494	0.721722 ± 10	0.70895	6.45	39.03	0.0999	0.511516 ± 10	− 7.2	7.9

$^{87}Sr/^{86}Sr$ and $^{143}Nd/^{144}Nd$ initial ratios were calculated for $T = 1.19$ Ga except for the BD_0 dike (GD 37) for which an age of 1.28 Ga (Upton et al., 2003) was assumed. Standard deviations for $\delta^{18}O$ are given for samples which were analyzed twice.

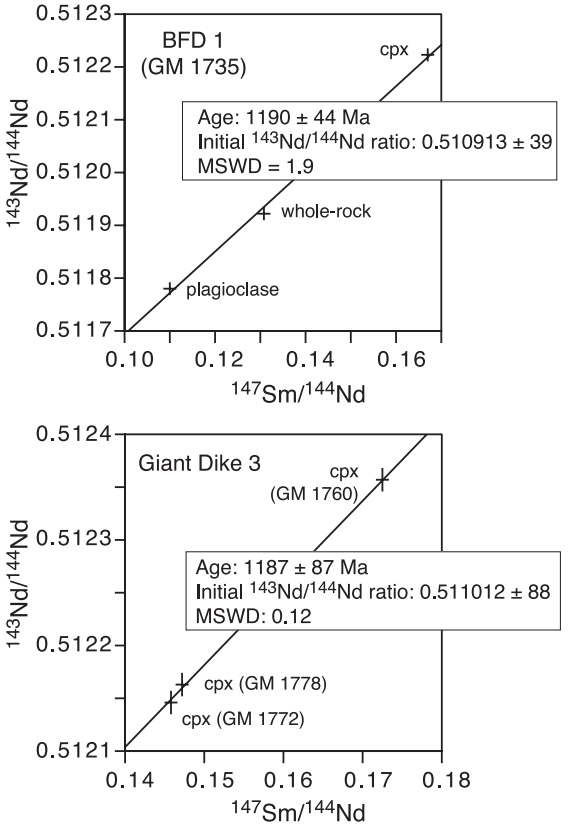

Fig. 11. Isochron diagrams for BFD 1 and Giant Dike 3. Error bars indicate 2σ errors. Errors used in the isochron calculations are $\pm 0.5\%$ for $^{147}Sm/^{144}Nd$ and 0.002% for $^{143}Nd/^{144}Nd$, based on repeated standard analyses. Isochrons were calculated after Wendt (1986).

basalts (Halama et al., 2003), but they do not reach the positive $\varepsilon_{Nd}(i)$ values of basaltic, lamprophyric and carbonatitic dikes from Ivittuut (Goodenough et al., 2002) and Igaliko (Pearce and Leng, 1996). The initial $^{87}Sr/^{86}Sr$ ratios of the Isortoq dikes, however, show a broad overlap with published data.

4.7. Re–Os isotopic analyses

The Os isotopic data presented in Table 9 include four samples from the Isortoq dike rocks together with four samples from the Eriksfjord Formation basalts (Halama et al., 2003) and two samples from the Ilímaussaq intrusion (Marks and Markl, 2001). The EF basalt samples were added to the data set because they represent even more primitive Gardar melts than the Isortoq dikes and are therefore more likely to reflect the Os isotopic composition of the mantle source. The augite–syenites from Ilímaussaq

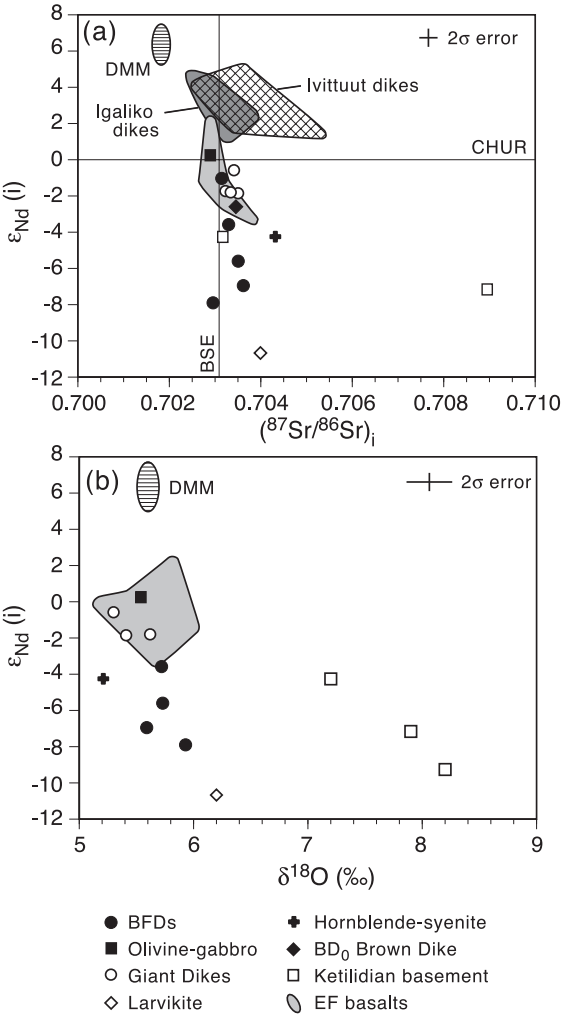

Fig. 12. (a) $\varepsilon_{Nd}(i)$ vs. $(^{87}Sr/^{86}Sr)_i$ diagram for mineral separates of Isortoq dike rocks and whole-rock basement samples. Reference data are from Pearce and Leng (1996), Goodenough et al. (2002) and Halama et al. (2003). The reference line of Bulk Silicate Earth (BSE) for the Sr isotopic composition was calculated after DePaolo (1988) assuming present-day values of 0.0827 for $^{87}Rb/^{86}Sr$ and 0.7045 for $^{87}Sr/^{86}Sr$. (b) Oxygen isotopic compositions vs. $\varepsilon_{Nd}(i)$ of separated clinopyroxenes and amphiboles from Isortoq dike rocks and whole-rock country rock samples. Oxygen isotopic composition of clinopyroxene from a DMM source was modeled using an average mantle olivine $\delta^{18}O$ value of 5.2‰ (Eiler et al., 1997) and an average $\Delta^{18}O_{cpx\text{-}olivine}$ fractionation of 0.4‰ (Mattey et al., 1994).

Table 9
Os isotope data of Isortoq dike rocks, Eriksfjord Formation basalts and Ilímaussaq syenites

Rock type	Sample	Age (Ma)[a]	Re (ng/g)	Os (ng/g)	Re/Os	$^{187}Re/^{188}Os$	$^{187}Os/^{188}Os$	$(^{187}Os/^{188}Os)_i$
Isortoq dikes								
BFD 1	GM 1735	1190	0.353	0.0153	23.13	176.44	4.6635 ± 89	1.131
GD 3, gabbro	GM 1760	1190	0.479	0.0070	68.74	4775.09	103.58 ± 16	7.967
Olivine–gabbro	GM 1803	1190	0.153	0.0021	71.71	2237.83	42.381 ± 58	−2.428
BFD 4	GD 39	1190	0.388	0.0144	26.86	213.58	5.181 ± 11	0.905
Eriksfjord formation basalts								
Basalt, Mussartût group	EF 024	1200	0.362	0.1490	2.43	11.60	0.10690 ± 1	−0.127
Basalt, Ulukasik group	EF 072	1200	0.343	0.0132	25.94	192.34	4.3238 ± 85	0.440
Basalt, Ilímaussaq group	EF 174	1200	0.207	0.0094	22.13	197.13	6.709 ± 21	2.729
Basalt, Ilímaussaq group	EF 168	1200	0.177	0.0123	14.45	93.49	2.8124 ± 61	0.925
Ilímaussaq intrusion								
Augite–syenite (center)	GM 1857	1160	0.013	0.0041	3.23	17.20	0.9751 ± 24	0.639
Augite–syenite (border)	GM 1858	1160	0.0026	0.00023	11.28	68.22	2.1395 ± 32	0.808

[a] Age determinations from Paslick et al. (2003) for the Eriksfjord Formation basalts and Waight et al. (2002) for the Ilímaussaq intrusion.

are the most primitive rocks of one of the major igneous complexes of the Gardar Province. Obtaining reliable geochemical information of these samples proved to be a challenging task because of the very low Os abundances and the potential Re mobility during secondary alteration, although it has been shown that the Re–Os system can remain resistant during low-degree metamorphism and hydrothermal alteration (Puchtel et al., 1999). One sample (EF 024) was omitted from data analysis because it was overspiked with respect to Os. The other samples show highly variable initial $^{187}Os/^{188}Os$ ratios ranging from −2.428 to 7.967 (Table 9). The negative $(^{187}Os/^{188}Os)_i$ of the olivine–gabbro is probably due to either analytical problems or mobilization of Re. All other $(^{187}Os/^{188}Os)_i$ values are much higher than those assumed for the various mantle components (0.105 − 0.152; Shirey and Walker, 1998). The initial $^{187}Os/^{188}Os$ ratio of the two most radiogenic samples are significantly higher than the estimated average upper crustal value of 1.9256 (Esser and Turekian, 1993) and a range of values from 0.1652 to 1.8138 for lower crustal xenoliths (Saal et al., 1998).

4.8. Oxygen isotope measurements

Oxygen isotope analyses of mineral separates from the dikes and whole-rock powders from the basement rocks are listed in Table 8. $\delta^{18}O$ values of clinopyroxene and amphibole separates from the dikes range from 5.2‰ to 6.2‰. The BFDs show a restricted range in $\delta^{18}O_{cpx}$ from 5.6‰ to 5.9‰ whereas the dikes without feldspathic material, i.e., the olivine–gabbro and the Giant Dikes, have lower $\delta^{18}O_{cpx}$ values in the range 5.3–5.6‰ . Most of the $\delta^{18}O_{cpx}$ values from the Isortoq dike swarm overlap with $\delta^{18}O_{cpx}$ values of mantle peridotites (5.25–5.90‰, Mattey et al., 1994), OIBs (5.3–6.1‰, Harris et al., 2000) and the spatially associated Eriksfjord Formation basalts (5.2–6.0‰, Halama et al., 2003).

The oxygen isotope equilibration temperature for fractionation between plagioclase and diopside was calculated after Zheng (1993) for sample GM 1735 (BFD 1) using Δ(plagioclase–diopside) = 0.89 and $X_{An} = 0.50$. The apparent equilibration temperature is 924 °C. Allowing an error of ± 0.15‰ in Δ, calculated temperatures range from 832 to 1035 °C. This indicates that the equilibration of oxygen isotopes occurred at magmatic temperatures.

Mineral melt fractionations allow the calculation of the magma oxygen isotopic compositions directly from measured values of minerals (Taylor and Sheppard, 1986). Using a $\Delta_{melt\text{-}cpx}$ value of 0.3, calculated after Kalamarides (1986) for a liquidus temperature of ~ 1130 °C, calculated $\delta^{18}O_{melt}$ values for the Isortoq dike rocks range from 5.5‰ to 6.5‰.

On the $\varepsilon_{Nd}(i)$–$\delta^{18}O$ diagram (Fig. 12b), the Isortoq dike rocks define a weak trend of slightly

increasing $\delta^{18}O$ with decreasing $\varepsilon_{Nd}(i)$. This trend does not approach the trend defined by the Ketilidian basement rocks. Some of the data overlap with comparative data from the Eriksfjord Formation basalts, but none of the Isortoq data plots close to a modeled DMM source.

5. Discussion

5.1. Validity of calculations of intrinsic parameters

Liquidus temperatures calculated for the Isortoq dike samples after Sugawara (2000) (1120–1145 °C) are in agreement with experimental results from Upton (1971) and Upton and Thomas (1980), who obtained liquidus temperatures of about 1190 °C for very similar gabbroic rocks from the Tugtutoq area and assumed that the intrusion of the dike magmas took place between 1160 and 1125 °C. Toplis and Carroll (1995) obtained similar liquidus temperatures for ferro-basaltic melts of ~1160 °C. Minimum crystallization temperatures derived from ternary feldspars yield temperatures in the range 950–1020 °C similar to intrusion temperatures of 1050 °C inferred for more differentiated syenitic rock types (Upton and Thomas, 1980).

Temperatures determined by QUILF (Andersen et al., 1993) can be subjected to subsolidus exchange (Markl et al., 1998) or they might reflect equilibration with a cooler, more fractionated residual melt because Fe/Mg silicates equilibrate fast when liquid is present (Markl and White, 1999). Our QUILF-calculated temperatures (930–850 °C) are slightly lower compared to solidus temperatures of hawaiitic magmas (990–965 °C, Upton, 1971). Therefore, QUILF temperatures calculated here are believed to reflect partly solidus temperatures and partly subsolidus exchange temperatures. Thus, the crystallization interval for the gabbroic rocks is assumed to be 1150–900 °C, whereas the syenitic rocks probably crystallized between 1050 and 800 °C.

The calculated silica activities correlate positively with whole-rock SiO_2 contents, indicating that the results are reliable. Oxygen fugacities indicate conditions below the FMQ buffer curve within the range of other Gardar magmas. Low oxygen fugacities appear to be a general feature of the Gardar magmas (Powell, 1978; Upton and Thomas, 1980; Larsen and Sørensen, 1987; Marks and Markl, 2001; Marks et al., 2003). Albeit the range in calculated $\log f_{O2}$ values is relatively large, there appears to be a general tendency of increasing oxygen fugacity with increasing silica activity (Fig. 7), which is confirmed by magnetite overgrowths over ilmenite in the larvikite. This feature may hint at an FMQ-type equilibrium buffering these parameters.

5.2. Evidence for closed-system fractionation in the giant dikes

The systematic decrease of X_{Fo} in olivine and X_{An} in plagioclase parallel to the assumed crystallization direction from the margin towards the dike center in GD 3 is interpreted to reflect fractional crystallization in an essentially closed system for the gabbroic facies of the dike. For various intrusions of the Gardar Province, in situ differentiation (e.g., Stephenson and Upton, 1982; Marks and Markl, 2001) and side-wall crystallization (e.g., Parsons and Brown, 1988) have been proposed as crystallization processes and it seems likely that both of those processes governed the magmatic evolution of the gabbroic facies of the Giant Dikes. Whole-rock geochemical data trends and REE patterns from clinopyroxenes are consistent with a closed-system fractional crystallization in Giant Dike 3. The Nd isotopic data provide evidence that fractionation from gabbroic to syenitic rocks in GD3 took place in a closed-system because the three samples from GD3 do not show any change in $\varepsilon_{Nd}(i)$ at various concentrations of SiO_2 (Fig. 13) and it was demonstrated earlier that they define an isochron age. Thus, the syenitic rocks may represent a more differentiated member of the same parental melt as the gabbroic rocks. However, differentiation did probably not occur in situ as field evidence (Bridgwater and Coe, 1970, and own observations) indicates that stoping was an important emplacement mechanism in the Giant Dikes. Possibly, Fe-rich and partly resorbed cores (Fig. 5) of augites from syenitic samples represent relics of crystals from partly solidified gabbroic rocks which where incorporated into the rising magma during emplacement of the syenitic members.

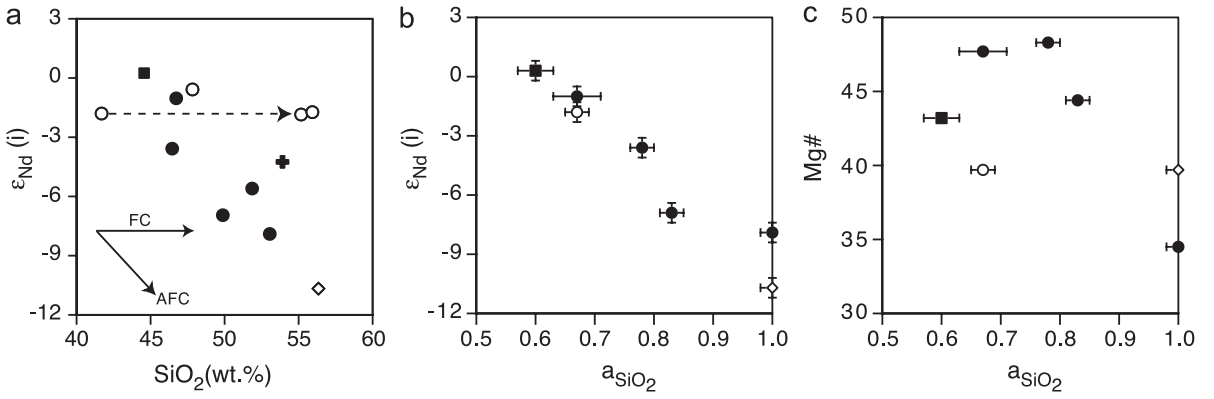

Fig. 13. (a) $\varepsilon_{Nd}(i)$ vs. SiO_2 (wt.%) diagram with general trends of fractional crystallization and AFC processes (solid arrows). Note the fractional crystallization trend for the three samples of Giant Dike 3 (dashed arrow). (b) and (c) Silica activities calculated with QUILF (Andersen et al., 1993) vs. $\varepsilon_{Nd}(i)$ and Mg# (symbols as in Fig. 12).

5.3. Evaluation of crustal contamination and mantle heterogeneity

Variations in the Sr–Nd isotopic composition of magmatic rocks can principally be explained by either crustal contamination or heterogeneous mantle sources. Today, the different mantle components have a wide range of isotopic compositions (Hart et al., 1992; Hofmann, 1997), but their projection into the Proterozoic is problematic. Generally speaking, steep trends on Sr–Nd isotope plots could be attributed to mixtures of an isotopically depleted mantle component and an isotopically enriched mantle component similar to EM-1 (e.g., Milner and Le Roex, 1996). The EM-1 component is characterized by extremely low $^{143}Nd/^{144}Nd$ ratios and negative ε_{Nd} values (Hofmann, 1997). Based on the Sr–Nd data alone, it seems possible that the dike magmas were derived from a source composed of two distinct mantle components, implying that the larvikite is closest to the EM-1-like end-member composition. However, mantle melts with these low initial Nd isotopic values are usually potassic, highly enriched in LREE and do not show any features indicative of crustal influences (e.g., Nelson, 1992; Schmidt et al., 1999). We will show below that there are many signs for a crustal component in the dike compositions and we therefore prefer the alternative view to explain the decrease in initial ε_{Nd} values by increasing amounts of crustal contamination (e.g., Paces and Bell, 1989).

In the Isortoq dikes, the rough negative correlation of a_{SiO2} with Mg# indicates that a_{SiO2} was increasing with fractionation and/or crustal contamination (Fig. 13). One possibility to explain this is that the liquid composition for the dike rocks started on the right-hand side of the thermal boundary in the nepheline–albite–quartz system, and therefore differentiation produced quartz-saturated compositions. However, the trend towards higher a_{SiO2} in the Isortoq dikes is not continuous as the most fractionated syenites of Giant Dike 3 are still below SiO_2 saturation, whereas the less fractionated larvikite contains quartz. The negative correlation of a_{SiO2} with ε_{Nd} (Fig. 13) is not compatible with simple fractionation trends, but suggests assimilation of relatively quartz-rich partial melts of crustal rocks that influenced the silica activities in the dikes to different degrees. Normative rock compositions agree well with the Nd isotope and QUILF data. Those rocks with relatively high ε_{Nd} are *ne*-normative, whereas the larvikite with the most negative ε_{Nd} is *qz*-normative, again consistent with assimilation of a SiO_2-rich partial melt. Mixing with SiO_2-rich mantle material is considered as unlikely because typical mantle-derived melts are usually poor in SiO_2 compared to crustal melts.

Geochemical data are in agreement with the assimilation hypothesis. High Ba contents typical of the Isortoq dikes (Fig. 10) resemble those in basaltic-hawaiitic lavas from Mull (Kerr et al., 1995). Based on melting experiments (Thompson, 1981), the latter were explained by addition partial melts derived from

Lewisian gneisses containing alkali feldspar as a source of the Ba (Kerr et al., 1995). This scenario is also conceivable for the Isortoq magmas when we consider contamination with Archean lithologies, which are present in the craton of southern West Greenland. There, granodioritic K-feldspar-bearing gneisses are quite common (McGregor, 1973; O'Nions and Pankhurst, 1974) and some of the gneisses are relatively Ba-rich (McGregor, 1979). Small negative Nb and Ti anomalies (Fig. 10) are consistent with contamination by crustal material modified or generated by subduction zone magmatism. In fact, they are typical features of Archean granulites (Rudnick and Presper, 1990) and negative Nb anomalies in flood basalts were previously explained by crustal contamination (McDonough, 1990). However, the presence of a negative Nb anomaly is no unequivocal evidence for crustal contamination, as it was also proposed to be characteristic for magmas derived from the SCLM (e.g., Hawkesworth et al., 1992; Goodenough et al., 2002).

Recent studies have shown that the Re–Os isotopic system can be a powerful tool to decipher crustal assimilation (e.g., Chesley and Ruiz, 1998) as some portions of the lower crust comprise the most radiogenic large-scale Os reservoirs within the Earth (Asmerom and Walker, 1998). Os concentrations in the Isortoq dike rocks are very low, probably because of the compatible behavior of Os during mantle melting (Shirey and Walker, 1998), prior sulfide separation and/or Os compatibility in olivine (Brügmann et al., 1987). Therefore, small amounts of crustal contamination may have a large impact on the Os isotopic composition of the magmas. On the Re–Os isochron diagram, the data points have a tendency to scatter around the 1.2 Ga reference line which is an approximate realistic age for all samples (Fig. 14). Excluding the relatively most altered Eriksf-

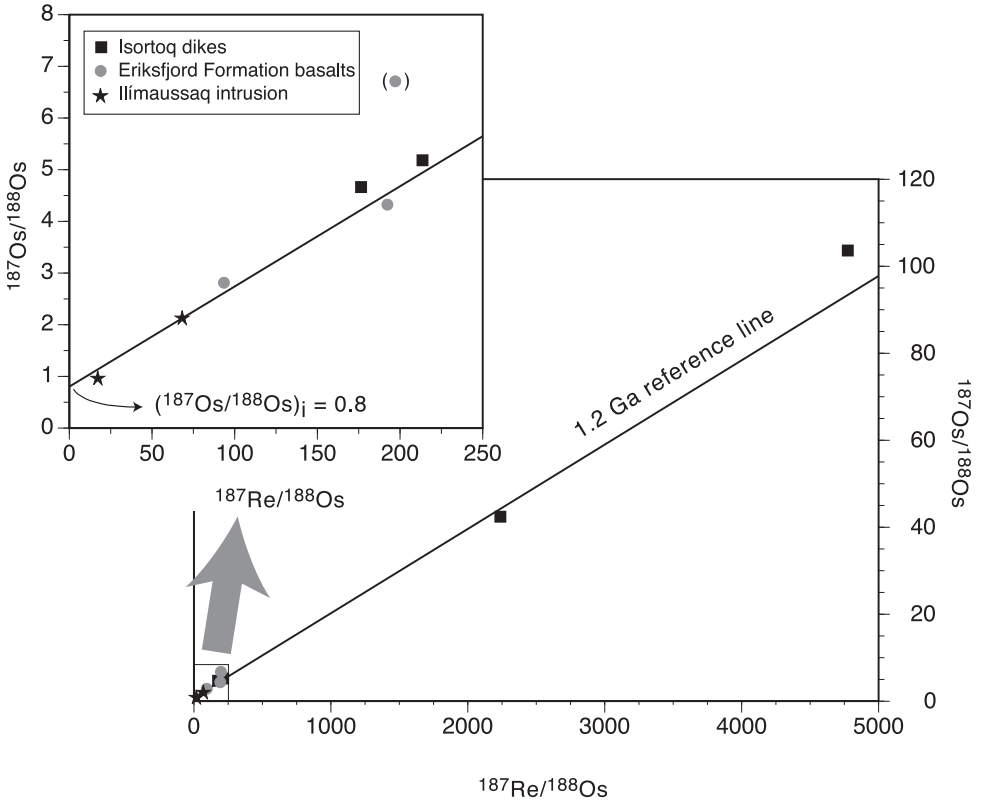

Fig. 14. Re–Os isotope composition correlation diagram for four Isortoq dikes, three Eriksfjord Formation basalts and two Ilímaussaq augite–syenites. Typical errors of 1 % for $^{187}Re/^{188}Os$ and 0.5 % for $^{187}Os/^{188}Os$ are smaller than the symbol size.

jord Formation basalt sample (EF 174), a reasonable fit of the reference line to the data points yields an initial $^{187}Os/^{188}Os$ ratio of ~ 0.8. Despite the large uncertainty in this estimation, this ratio is much higher than $^{187}Os/^{188}Os$ values of all known mantle reservoirs (Shirey and Walker, 1998). Therefore, the Os isotopic composition does not reflect a primary mantle composition. The only reservoir known to contain significant radiogenic Os is old continental crust (Chesley and Ruiz, 1998) and lower crustal xenoliths with $^{187}Os/^{188}Os$ values as high as 3.5 have been reported (Molzahn et al., 1996). Accordingly, several studies postulated the assimilation of material from the lower crust in the petrogenesis of mafic continental magmas (e.g., Asmerom and Walker, 1998; Sproule et al., 2002). The Os isotopic data are at least compatible with an important role of assimilation of crustal material in the petrogenesis of the Gardar magmas. The high initial $^{187}Os/^{188}Os$ ratio might suggest that almost all Os was crustally derived.

Fractionation of olivine, clinopyroxene, plagioclase and Fe–Ti oxides is known to produce small increases in melt $\delta^{18}O$ values (< 0.3 ‰) and the increase in the $\Delta_{melt\text{-}cpx}$ fractionation factor with decreasing T is about 0.1 ‰ in $\delta^{18}O$ of the clinopyroxene (Baker et al., 2000). Therefore, these processes can only partly account for the increase in $\delta^{18}O$ isotopic values in the Isortoq clinopyroxenes. Because the EM-1 mantle component does not deviate significantly from average upper mantle values (Eiler et al., 1997), the $\delta^{18}O_{melt}$ in the larvikite is above typical values for mantle melts and requires another explanation than a heterogeneous mantle source. The weak positive correlations of $\delta^{18}O$ with ε_{Nd} (Fig. 12b) and Eu/Eu^*_{cpx} (Fig. 15) are consistent with an $\delta^{18}O$ increase due to crustal contamination. The Nd–O data indicate that assimilation of Ketilidian upper crustal basement is unlikely (Fig. 12b). This is supported by field evidence as granitoid xenoliths in the dikes are characterized by sharp contacts, suggesting that they did not react much with the magmas. Lower crustal rocks of igneous origin have an average $\delta^{18}O$ value of + 7.5 ± 1.4 ‰ with an overall range from + 5.4 ‰ to + 12.5 ‰ (Fowler and Harmon, 1990) and contamination with crustal material with oxygen isotopic values of + 7.0 ‰ to + 10 ‰ and low ε_{Nd} values is in qualitative agreement with the data.

Having established that the olivine–gabbro and the Giant Dikes are less crustally contaminated than the BFDs, the absence of a negative Eu anomaly in the BFDs needs to be explained. Intuitively, one would expect that the more pronounced the influence of the AFC process is, the larger should the negative Eu anomaly be. However, this is not the case and alternative explanations are required. A significant difference in the oxidation state of the magmas can be excluded

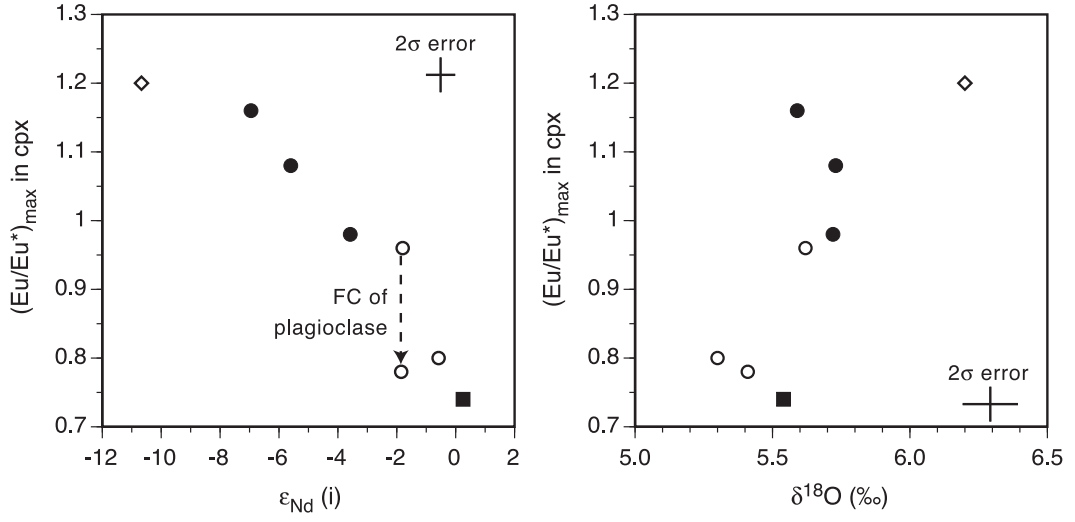

Fig. 15. Maximum Eu anomalies in clinopyroxenes from Isortoq dike rocks vs. $\varepsilon_{Nd}(i)$ and $\delta^{18}O$ (symbols as in Fig. 12). The assumed 2σ error for Eu/Eu* is ± 0.05.

because QUILF calculations show negative ΔFMQ values for both. A more viable explanation for the lack of negative Eu anomalies in the BFD clinopyroxenes is resorption of plagioclase in the melt either due to a pressure decrease or due to injection of new, hot magma (Markl and Frost, 1999). BFD magmas could have been mechanically enriched in plagioclase in a magma chamber possibly close to the crust–mantle boundary before the resorption started. Alternatively, interaction with lower crust can even produce positive Eu anomalies in the melts (Mitchell et al., 1995). This explanation is also compatible with the negative correlation of Eu/Eu^*_{max} with ε_{Nd} (Fig. 15) because a larger degree of assimilation as seen in the BFDs would also lead to a relative enrichment in Eu. REE data of amphibolite- and granulite-facies gneisses from the Archean craton of southern West Greenland frequently show a prominent positive Eu anomaly (Compton, 1978) and contamination of the dike magmas with similar material is therefore in agreement with the REE data.

5.4. Quantitative modeling of crustal contamination processes

Mechanisms to explain contamination signatures in mantle-derived mafic magmas include assimilation coupled with fractional crystallization (AFC) (Bowen, 1928; Taylor, 1980; DePaolo, 1981) and assimilation of crust by the most mafic magmas during turbulent ascent (ATA) (Huppert and Sparks, 1985; Devey and Cox, 1987). Correlations of isotopic ratios and parameters of fractionation can be used to evaluate which process is more likely to have occurred. For the Isortoq magmas, the $\varepsilon_{Nd}(i)$ vs. SiO_2 diagram (Fig. 13) reveals a negative correlation. This indicates that AFC processes were operating because AFC processes result in the most evolved rocks becoming the most contaminated. Quantification of the AFC processes was carried out using an energy-constrained assimilation-fractional crystallization (EC-AFC) model (Spera and Bohrson, 2001; Bohrson and Spera, 2001). Because some of the trace elements analyzed are prone to mobilization (Rb, Ba, K) or influenced by accumulation or fractionation processes (P, Ti, Sr) and the oxygen isotope data show only a limited spread, we constrained this modeling to the Sr–Nd isotopic compositions.

Several studies proposed assimilation of granulite facies gneisses by mafic magmas to explain steep trends on Sr–Nd isotope diagrams (e.g., Carter et al., 1978; Bernstein et al., 1998). A negative correlation between ε_{Nd} and SiO_2 content was suggested as further indication for assimilation of Archean granulite-facies lower crust (Heaman and Machado, 1992). Because our data point towards compositionally similar contaminants and seismic data were interpreted to reflect the existence of a wedge of Archean crust that extends southwards to Lindenow Fjord (Dahl-Jensen et al., 1998), we used an average of five granulite-facies gneisses with low Rb/Sr ratios from the Archean craton of West Greenland (Taylor et al., 1984) as representative for the lower crustal composition (Table 10). The Julianehåb granitoids, in which the dikes were emplaced and which represents the most abundant country rock, are a second possible contaminant. Thus, the weighted

Table 10
Parameters used in energy-constrained assimilation-fractional crystallization (EC-AFC) modeling

Thermal parameters:		
Liquidus temperature of magma (°C)	1190	
Initial temperature of magma (°C)	1140	
Solidus temperature (°C)	850	
Temperature of equilibration (°C)	900	
Compositional parameters:	**Sr**	**Nd**
Magma initial concentration (ppm)	411	32
Magma isotope ratio	0.70289	0.51111
Magma trace element distribution coefficient	1.5	0.25
Upper crustal assimilant initial concentration (ppm)	480	35
Upper crustal assimilant isotope ratio	0.70806	0.51069
Lower crustal assimilant initial concentration (ppm)	747	63
Lower crustal assimilant isotope ratio	0.70670	0.5099
Assimilant trace element distribution coefficient	1.5	0.25

For the upper and lower crustal assimilants, the thermal parameters for the "standard" upper crustal and the "standard" lower crustal case, respectively, were taken from Bohrson and Spera (2001).

average from the three granitoid samples of the Julianehåb batholith were used as representative for the chemical composition of an upper crustal contaminant. Sr is modeled as compatible in the assimilant because the assimilated material is thought to be plagioclase-rich based on the ε_{Nd}–Eu/Eu$^*_{max}$ correlation (Fig. 15). In the magma, Sr is also modeled as slightly compatible consistent with the influence of plagioclase on the fractionating assemblage. Following Bohrson and Spera (2001), Nd is modeled as incompatible both in the magma and the upper and lower crustal assimilants.

The results indicate that AFC processes involving upper crustal Ketilidian basement cannot explain the steep trend on the Sr–Nd isotope diagram, although an upper crustal component appears to be involved in the petrogenesis of the hornblende–syenite (Fig. 16). On the other hand, assimilation of lower crustal material is consistent with the bulk of the data and indicates a maximum mass of assimilated anatectic melt of ~ 10% (Fig. 16). However, the starting composition, chosen to be similar to the isotopically most primitive samples, might already be contaminated by some crustal material and therefore 10% is not a maximum value. We

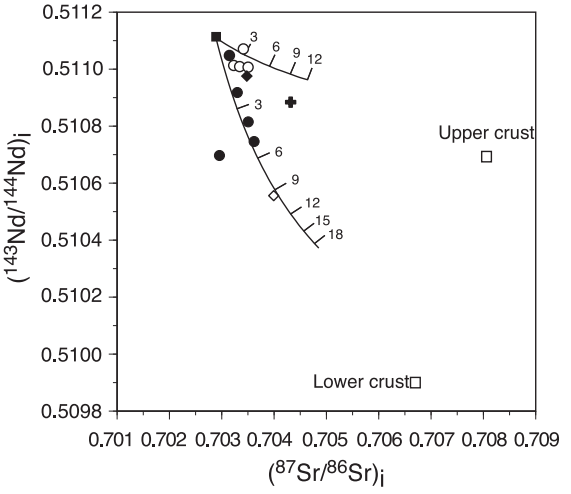

Fig. 16. Sr–Nd isotope diagram showing the results of the AFC modeling with the parameters from Table 10 (symbols as in Fig. 12). Isotopic compositions of upper crust is an weighted average from the three basement samples and lower crust is represented by an average of five Archean granulite facies gneisses with low Rb/Sr ratios from Taylor et al. (1984). Numbers at EC-AFC curves indicate the percentage of mass of assimilated partial melt.

conclude that AFC processes involving magmas isotopically similar to the most primitive of the Isortoq dikes and up to ~ 10% partial melts derived from lower crustal rocks similar to Archean granulite-facies gneisses can reasonably explain the bulk of the Sr–Nd isotope data. The hornblende–syenite appears to be contaminated with both upper and lower crustal material, whereas the off-trend position of BFD 2 can be explained by assimilation of isotopically and/or chemically heterogeneous material.

5.5. Regional perspective

Contamination of Gardar magmas with crustal rocks was demonstrated previously at several localities (e.g., Taylor and Upton, 1993; Andersen, 1997; Stevenson et al., 1997; Marks and Markl, 2001). However, there has been no consensus whether the Ketilidian mobile belt, in which the Isortoq dikes are emplaced, is underlain by Archean crust. This hypothesis was rejected based on isotopic and geochemical data of the Ketilidian granites (van Bremen et al., 1974; Kalsbeek and Taylor, 1985), although field evidence suggested the presence of older basement in the mobile belt (van Bremen et al., 1974). On the other hand, seismic data indicate that a wedge of Archean crust underlies the predominant part of the Ketilidian belt (Dahl-Jensen et al., 1998) and recent studies on Gardar rocks suggest an involvement of lower crustal material in their petrogenesis (Marks et al., 2003; Halama et al., 2003). The ε_{Nd} data reported here are among the most negative for Gardar rocks and together with petrological and Sr–O–Os isotopic data provide compelling evidence for assimilation of partial melts from lower crustal rocks similar to granulite-facies gneisses from the Archean craton. A Pb isotope study is planed to further elucidate the extent of Archean crust below South Greenland. For the anorthosite xenolith, it is noteworthy that the REE patterns of the clinopyroxenes and the strongly negative ε_{Nd} value are compatible with a significant input of crustal partial melts. This is in contrast to previous observations which concluded, based on the alkalic character of the anorthosites and the low initial $^{87}Sr/^{86}Sr$ values, that crustal assimilation was insignificant in the formation of the anorthositic rocks (Patchett et al., 1976). On the other hand, the data from Giant Dike 3 show that closed-system fractional

crystallization operated at near-surface levels in magmas that were contaminated prior to emplacement.

6. Conclusions

The importance of mafic rocks as probes of the continental crust they have traversed rather than as probes of the lithospheric mantle was recently stressed by Baker et al. (1998). Our data of the Isortoq dikes indicate that the assimilated material must have been silicic because the increase in a_{SiO2} and SiO_2 content in some dikes is higher than expected from fractional crystallization alone. REE and Nd isotopic data require the assimilated material to be rich in plagioclase component. Isotopic characteristics of the crustal component include a very low $^{143}Nd/^{144}Nd$ and a moderately low $^{87}Sr/^{86}Sr$ ratio. Furthermore, low Nb contents, moderate $\delta^{18}O$ values and a highly radiogenic Os isotopic composition of the assimilant are indicated. All these features are compatible with assimilation of partial melts derived from Archean granulite-facies gneisses similar to those present in the Archean craton north of the Ketilidian mobile belt. In agreement with seismic data (Dahl-Jensen et al., 1998), we therefore suggest that Archean rocks occur at depth in the Isortoq region, thus continuing further south than at the present erosion level. Assimilation of upper crustal material was generally insignificant, but might have operated in the petrogenesis of the hornblende–syenite dike.

Due to their crustal contamination, mantle source characteristics of the Isortoq dikes are masked. However, the general relative enrichment in incompatible elements and the Sr–Nd isotopic compositions argue against a significant role of depleted MORB mantle in the magma generation. The clinopyroxene REE patterns do also not show any similarity to patterns from MORB-like gabbros, but they are very similar to patterns from cumulus clinopyroxene in gabbroic rocks related to postbreakup magmatism caused by the proximity of the Iceland plume in East Greenland (Bernstein et al., 1998). However, the importance of crustal contamination demonstrated for the Isortoq dikes makes it impossible to distinguish whether the enrichment in incompatible trace elements relative to the primitive mantle was derived from the SCLM, an enriched plume or a mixture of both.

Acknowledgements

We would like to thank Bruce Paterson who provided invaluable help during Laser ICP-MS measurements at the Large-Scale Geochemical Facility supported by the European Community-Access to Research Infrastructure action of the Improving Human Potential Programme, contract number HPRI-CT-1999-00008 awarded to Prof. B.J. Wood (University of Bristol). Gabi Stoschek and Torsten Vennemann are thanked for their help with oxygen isotope measurements. Elmar Reitter expertly assisted with preparation and measurements of radiogenic isotopes and Mathias Westphal helped with microprobe measurements. Constructive reviews by S. Bernstein and G. Fitton greatly improved the manuscript. Financial funding of this work by the Deutsche Forschungsgemeinschaft (grant Ma-2135/1-2) is gratefully acknowledged.

References

Allaart, J.H., 1976. Ketilidian mobile belt in South Greenland. In: Escher, A., Watt, W.S. (Eds.), Geology of Greenland. Grønlands Geologiske Undersøgelse, Copenhagen, pp. 121–151.

Andersen, T., 1997. Age and petrogenesis of the Qassiarsuk carbonatite–alkaline silicate volcanic complex in the Gardar rift, South Greenland. Mineralogical Magazine 61, 499–513.

Andersen, D.J., Lindsley, D.H., Davidson, P.M., 1993. QUILF: a PASCAL program to assess equilibria among Fe–Mg–Mn–Ti oxides, pyroxenes, olivine, and quartz. Computers & Geosciences 19, 1333–1350.

Armstrong, J.T., 1991. Quantitative elemental analysis of individual microparticles with electron beam instruments. In: Heinrich, K.F.J., Newbury, D.E. (Eds.), Electron Probe Quantitation. Plenum, New York, pp. 261–315.

Asmerom, Y., Walker, R.J., 1998. Pb and Os isotopic constraints on the composition and rheology of the lower crust. Geology 26, 359–362.

Baker, J.A., Menzies, M.A., Thirlwall, M.F., Macpherson, C.G., 1998. Petrogenesis of quaternary intraplate volcanism, Sana'a, Yemen: implications for plume–lithosphere interaction and polybaric melt hybridization. Journal of Petrology 38, 1359–1390.

Baker, J.A., MacPherson, C.G., Menzies, M.A., Thirlwall, M.F., Al-Kadasi, M., Mattey, D.P., 2000. Resolving crustal and mantle contributions to continental flood volcanism, Yemen; constraints from mineral oxygen isotope data. Journal of Petrology 41, 1805–1820.

Benoit, M., Polvé, M., Ceuleneer, G., 1996. Trace element and isotopic characterization of mafic cumulates in a fossil mantle diapir (Oman ophiolite). Chemical Geology 134, 199–214.

Bernstein, S., Kelemen, P.B., Tegner, C., Kurz, M.D., Blusztajn, J., Kent Brooks, C., 1998. Post-breakup basaltic magmatism along the East Greenland Tertiary rifted margin. Earth and Planetary Science Letters 160, 845–862.

Birck, J.L., Roy Barman, M., Capmas, F., 1997. Re–Os isotopic measurements at the femtomole level in natural samples. Geostandards Newsletter 20, 19–27.

Bohrson, W.A., Spera, F.J., 2001. Energy-constrained open-system magmatic processes: II. Application of energy-constrained assimilation-fractional crystallization (EC-AFC) model to magmatic systems. Journal of Petrology 42, 1019–1041.

Boily, M., Ludden, J.N., 1991. Trace-element and Nd isotopic variations in Early Proterozoic dyke swarms emplaced in the vicinity of the Kapuskasing structural zone: enriched mantle or assimilation and fractional crystallization (AFC) process? Canadian Journal of Earth Sciences 28, 26–36.

Bowen, N.L., 1928. The Evolution of the Igneous Rocks. Princeton Univ. Press, Princeton 332 pp.

Boynton, W.V., 1984. Geochemistry of the rare earth elements: meteorite studies. In: Henderson, P. (Ed.), Rare Earth Element Geochemistry. Elsevier, Amsterdam, pp. 63–114.

Bridgwater, D., 1967. Feldspathic inclusions in the Gardar igneous rocks of South Greenland and their relevance to the formation of major anorthosites in the Canadian Shield. Canadian Journal of Earth Sciences 4, 995–1014.

Bridgwater, D., Coe, K., 1970. The role of stoping in the emplacement of the giant dikes of Isortoq, South Greenland. Geological Journal 2, 67–78 (special issue).

Bridgwater, D., Harry, W.T., 1968. Anorthosite xenoliths and plagioclase megacrysts in Precambrian intrusions of South Greenland. Meddelelser om Grønland, 185.

Brügmann, G.E., Arndt, N.T., Hofmann, A.W., Tobschall, H.J., 1987. Noble metal abundances in komatiite suites from Alexo, Ontario and Gorgona Island, Columbia. Geochimica et Cosmochimica Acta 51, 2159–2169.

Buddington, A.F., Lindsley, D.H., 1964. Iron–titanium oxide minerals and synthetic equivalents. Journal of Petrology 5, 310–357.

Carter, S.R., Evensen, N.M., Hamilton, P.J., O'Nions, R.K., 1978. Neodymium and strontium isotope evidence for crustal contamination of continental volcanics. Science 202, 743–747.

Chesley, J.T., Ruiz, J., 1998. Crust–mantle interaction in large igneous provinces: implications from the Re–Os isotope systematics of the Columbia River flood basalts. Earth and Planetary Science Letters 154, 1–11.

Class, C., Altherr, R., Volker, F., Eberz, G., McCulloch, M.T., 1994. Geochemistry of Pliocene to Quarternary alkali basalts from the Huri Hills, northern Kenya. Chemical Geology 113, 1–22.

Clayton, R.N., Mayeda, T.K., 1963. The use of bromine pentafluoride in the extraction of oxygen from oxides and silicates for isotope analysis. Geochimica et Cosmochimica Acta 27, 43–52.

Compton, P., 1978. Rare earth evidence for the origin of the Nûk Gneisses, Buksefjorden Region, Southern West Greenland. Contributions to Mineralogy and Petrology 66, 283–293.

Condie, K.C., Bobrow, D.J., Card, K.D., 1987. Geochemistry of Precambrian mafic dykes from the Southern Superior Province of the Canadian Shield. In: Halls, H.C., Fahrig, W.C. (Eds.), Mafic Dyke SwarmsSpecial Publication-Geological Association of Canada, vol. 34, pp. 95–107.

Cox, K.G., Bell, J.D., Pankhurst, R.J., 1979. The Interpretation of Igneous Rocks. George, Allen and Unwin, London.

Cross, W., Iddings, J.P., Pirsson, L.V., Washington, H.S., 1903. Quantitative Classification of Igneous Rocks. University of Chicago Press, Chicago.

Dahl-Jensen, T., Thybo, T., Hopper, H., Rosing, M., 1998. Crustal structure at the SE Greenland margin from wide-angle and normal incidence seismic data. Tectonophysics 288, 191–198.

DePaolo, D.J., 1981. Trace element and isotopic effects of combined wallrock assimilation and fractional crystallisation. Earth and Planetary Science Letters 53, 189–202.

DePaolo, D.J., 1988. Neodymium Isotope Geochemistry: An Introduction. Springer-Verlag, New York.

Devey, C.W., Cox, K.G., 1987. Relationships between crustal contamination and crystallisation in continental flood basalt magmas with special reference to the Deccan Traps of the Western Ghats, India. Earth and Planetary Science Letters 84, 59–68.

Eiler, J.M., Farley, K.A., Valley, J.W., Hauri, E., Craig, H., Hart, S.R., Stolper, E.M., 1997. Oxygen isotope variations in ocean island basalt phenocrysts. Geochimica et Cosmochimica Acta 61, 2281–2293.

Elkins, L.T., Grove, T.L., 1990. Ternary feldspar experiments and thermodynamic models. American Mineralogist 75, 544–559.

Ellam, R.M., Carlson, R.W., Shirey, S.B., 1992. Evidence from Re–Os isotopes for plume–lithosphere mixing in Karoo flood basalt genesis. Nature 359, 718–721.

Emeleus, C.H., Upton, B.G.J., 1976. The Gardar period in southern Greenland. In: Escher, A., Watt, W.S. (Eds.), Geology of Greenland. Geological Survey of Greenland, Copenhagen, pp. 152–181.

Engell, J., Pedersen, S., 1974. Rb–Sr whole rock isochron age determination from the Bangs Havn intrusion, South Greenland. Bulletin of the Geological Society of Denmark 23, 130–133.

Ernst, R.E., Buchan, K.L., 1997. Giant radiating dyke swarms: their use in identifying pre-Mesozoic large igneous provinces and mantle plumes. In: Mahoney, J.J., Coffin, M.E. (Eds.), Large Igneous Provinces: Continental, Oceanic, and Planetary Flood Volcanism. Geophysical Monograph, vol. 100, pp. 297–333.

Ernst, R.E., Buchan, K.L., 2001. The use of mafic dike swarms in identifying and locating mantle plumes. In: Ernst, R.E., Buchan, K.L. (Eds.), Mantle Plumes: Their Identification Through Time-Special Paper-Geological Society of America, vol. 352, pp. 247–265.

Esser, B.K., Turekian, K.K., 1993. The osmium isotopic composition of the continental crust. Geochimica et Cosmochimica Acta 57, 3093–3104.

Finch, A.A., Mansfeld, J., Andersen, T., 2001. U–Pb radiometric age of Nunarsuit pegmatite, Greenland: constraints on the timing of Gardar magmatism. Bulletin of the Geological Society of Denmark 48, 1–7.

Fowler, M.B., Harmon, R.S., 1990. The oxygen isotope composition of lower crustal granulite xenoliths. In: Vielzeuf, D., Vidal, P. (Eds.), Granulites and Crustal Evolution. Kluwer Academic Publishing, Dordrecht, pp. 493–506.

Frost, B.R., Lindsley, D.H., 1992. Equilibria among Fe–Ti-oxides,

pyroxenes, olivine, and quartz: Part II. Application. American Mineralogist 77, 1004–1020.

Gallagher, K., Hawkesworth, C., 1992. Dehydration melting and the generation of continental flood basalts. Nature 358, 57–59.

Garde, A.A., Hamilton, M.A., Chadwick, B., Grocott, J., McCaffrey, K.J.W., 2002. The Ketilidian orogen of South Greenland: geochronology, tectonics, magmatism, and fore-arc accretion during Palaeoproterozoic oblique convergence. Canadian Journal of Earth Sciences 39, 765–793.

Gibson, S.A., Thompson, R.N., Dickin, A.P., Leonardos, O.H., 1995. High-Ti and low-Ti mafic potassic magmas: key to plume–lithosphere interactions and continental flood-basalt genesis. Earth and Planetary Science Letters 136, 149–165.

Goldstein, S.L., O'Nions, R.K., Hamilton, P.J., 1984. A Sm–Nd isotopic study of the atmospheric dust and particulates from major river systems. Earth and Planetary Science Letters 70, 221–236.

Goodenough, K.M., Upton, B.G.J., Ellam, R.M., 2002. Long-term memory of subduction processes in the lithospheric mantle: evidence from the geochemistry of basic dykes in the Gardar Province of south Greenland. Journal of the Geological Society (London) 159, 705–714.

Halama, R., Waight, T., Markl, G., 2002. Geochemical and isotopic zoning patterns of plagioclase megacrysts in gabbroic dykes from the Gardar Province, South Greenland: implications for crystallisation processes in anorthositic magmas. Contributions to Mineralogy and Petrology 144, 109–127.

Halama, R., Wenzel, T., Upton, B.G.J., Siebel, W., Markl, G., 2003. A geochemical and Sr–Nd–O isotopic study of the Proterozoic Eriksfjord Basalts, Gardar Province, South Greenland: reconstruction of an OIB signature in crustally contaminated rift-related basalts. Mineralogical Magazine 67, 831–854.

Harris, C., Smith, H.S., le Roex, A.P., 2000. Oxygen isotope composition of phenocrysts from Tristan da Cunha and Gough Island lavas: variation with fractional crystallization and evidence for assimilation. Contributions to Mineralogy and Petrology 138, 164–175.

Hart, S.R., Hauri, E.H., Oschmann, L.A., Whitehead, J.A., 1992. Mantle plumes and entrainment: isotopic evidence. Science 256, 517–520.

Hawkesworth, C.J., Gallagher, K., Kelly, S., Mantovani, M., Peate, D.W., Regelous, M., Rogers, N.W., 1992. Paraná magmatism and the opening of the South Atlantic. In: Storey, B.C., Alabaster, T., Pankhurst, R.J. (Eds.), Magmatism and the Causes of Continental Break-upSpecial Publication-Geological Society of London, vol. 68, pp. 221–240.

Heaman, L.M., Machado, N., 1992. Timing and origin of midcontinent rift alkaline magmatism, North America: evidence from the Coldwell Complex. Contributions to Mineralogy and Petrology 110, 289–303.

Hofmann, A.W., 1997. Mantle geochemistry: the message from oceanic volcanism. Nature 385, 219–229.

Huppert, H.E., Sparks, R.S.J., 1985. Cooling and contamination of mafic and ultramafic magmas during ascent through continental crust. Earth and Planetary Science Letters 74, 371–386.

Jacobson, S.B., Wasserburg, G.J., 1980. Sm–Nd isotopic evolution of chondrites. Earth and Planetary Science Letters 50, 139–155.

Kalamarides, R.I., 1986. High-temperature oxygen isotope fractionation among the phases of Kiglapait intrusion, Labrador, Canada. Chemical Geology 58, 303–310.

Kalsbeek, F., Taylor, P.N., 1985. Isotopic and chemical variation in granites across a Proterozoic continental margin—the Ketilidian mobile belt of South Greenland. Earth and Planetary Science Letters 73, 65–80.

Kerr, A.C., Kempton, P.D., Thompson, R.N., 1995. Crustal assimilation during turbulent magma ascent (ATA); new isotopic evidence from the Mull Tertiary lava succession, N.W. Scotland. Contributions to Mineralogy and Petrology 119, 142–154.

Konnerup-Madsen, J., Rose-Hansen, J., 1984. Composition and significance of fluid inclusions in the Ilímaussaq peralkaline granite, South Greenland. Bulletin Minéralogique 107, 317–326.

Kretz, R., 1983. Symbols for rock-forming minerals. American Mineralogist 68, 277–279.

Larsen, L.M., Sørensen, H., 1987. The Ilimaussaq intrusion-progressive crystallization and formation of layering in an agpaitic magma. In: Fitton, J.G., Upton, B.G.J. (Eds.), Alkaline Igneous Rocks. Special Publication-Geological Society of London, vol. 30, pp. 473–488.

LeCheminant, A.N., Heaman, L.M., 1989. Mackenzie igneous events, Canada: Middle Proterozoic hotspot magmatism associated with ocean opening. Earth and Planetary Science Letters 96, 38–48.

Lightfoot, P.C., Sutcliffe, R.H., Doherty, W., 1991. Crustal contamination identified in Keweenawan Osler Group Tholeiites, Ontario: a trace element perspective. Journal of Geology 99, 739–760.

Lindsley, D.H., 1983. Pyroxene thermometry. American Mineralogist 68, 477–493.

Lindsley, D.H., Frost, B.R., 1992. Equilibria among Fe–Ti-oxides, pyroxenes, olivine, and quartz: Part I. Theory. American Mineralogist 77, 987–1003.

Markl, G., Frost, B.R., 1999. The origin of anorthosites and related rocks from the Lofoten Islands, Northern Norway: II. Calculation of parental liquid compositions for anorthosites. Journal of Petrology 40, 61–77.

Markl, G., White, C., 1999. Pigeonite–augite intergrowths from the Graveyard Point sill, Oregon: a record of the interplay between bulk and interstitial liquid fractionation. Contributions to Mineralogy and Petrology 137, 170–183.

Markl, G., Frost, B.R., Bucher, K., 1998. The origin of anorthosites and related rocks from the Lofoten islands, Northern Norway: I. Field relations and estimation of intrinsic variables. Journal of Petrology 39, 1425–1452.

Marks, M., Markl, G., 2001. Fractionation and assimilation processes in the alkaline augite syenite unit of the Ilimaussaq Intrusion, South Greenland, as deduced from phase equilibria. Journal of Petrology 42, 1947–1969.

Marks, M., Vennemann, T., Siebel, W., Markl, G., 2003. Quantification of magmatic and hydrothermal processes in a peralkaline syenite–alkali granite complex based on textures, phase equilibria, and stable and radiogenic isotopes. Journal of Petrology 44, 1247–1280.

Mattey, D., Lowry, D., Macpherson, C., 1994. Oxygen isotope

composition of mantle peridotite. Earth and Planetary Science Letters 128, 231–241.
McDonough, W.F., 1990. Constraints on the composition of the continental lithospheric mantle. Earth and Planetary Science Letters 101, 1–18.
McDonough, W.F., Sun, S.S., 1995. The composition of the Earth. Chemical Geology 120, 223–253.
McGregor, V.R., 1973. The early Precambrian gneisses of the Godthaab district, West Greenland. Philosophical Transactions of the Royal Society of London A273, 343–358.
McGregor, V.R., 1979. Archean gray gneisses and the origin of the continental crust; evidence from the Godthaab region, West Greenland. In: Barker, F. (Ed.), Trondhjemites, Dacites, and Related Rocks. Elsevier, Amsterdam, pp. 169–204.
Middlemost, E.A.K., 1989. Iron oxidation ratios, norms and the classification of volcanic rocks. Chemical Geology 77, 19–26.
Milner, S.C., Le Roex, A.P., 1996. Isotope characteristics of the Okenyenya igneous complex, northwestern Namibia: constraints on the composition of the early Tristan plume and the origin of the EM 1 mantle component. Earth and Planetary Science Letters 141, 277–291.
Mitchell, J.N., Scoates, J.S., Frost, C.D., 1995. High-Al gabbros in the Laramie Anorthosite Complex, Wyoming: implications for the composition of melts parental to Proterozoic anorthosite. Contributions to Mineralogy and Petrology 119, 166–180.
Mohr, P.A., 1987. Crustal Contamination in Mafic Sheets: a summary. In: Halls, H.C., Fahrig, W.C. (Eds.), Mafic Dyke Swarms. Special Publication-Geological Association of Canada, vol. 34, pp. 75–80.
Molzahn, M., Reisberg, L., Wörner, G., 1996. Os, Sr, Nd, Pb, O isotope and trace element data from the Ferrar flood basalts, Antarctica: evidence for an enriched subcontinental lithospheric source. Earth and Planetary Science Letters 144, 529–546.
Nelson, D.R., 1992. Isotopic characteristics of potassic rocks: evidence for the involvement of subducted sediments in magma genesis. Lithos 28, 403–420.
O'Hara, M.J., Herzberg, C., 2002. Interpretation of trace element and isotope features of basalts: relevance of field relations, petrology, major element data, phase equilibria, and magma chamber modeling in basalt petrogenesis. Geochimica et Cosmochimica Acta 66, 2167–2191.
O'Nions, R.K., Pankhurst, R.J., 1974. Rare-earth element distribution in Archaean gneisses and anorthosites, Godthåb area, West Greenland. Earth and Planetary Science Letters 22, 328–338.
Paces, J.B., Bell, K., 1989. Non-depleted sub-continental mantle beneath the Superior Province of the Canadian Shield: Nd–Sr isotopic and trace element evidence from Midcontinent Rift basalts. Geochimica et Cosmochimica Acta 53, 2023–2035.
Parsons, I., Brown, W.L., 1988. Sidewall crystallization in the Klokken intrusion: zoned ternary feldspars and coexisting minerals. Contributions to Mineralogy and Petrology 98, 431–443.
Paslick, C.R., Halliday, A.N., Davies, G.R., Mezger, K., Upton, B.G.J., 2003. Timing of proterozoic magmatism in the Gardar Province, Southern Greenland. Bulletin Geological Society of America 105, 272–278.
Patchett, J., Bridgwater, D., 1984. Origin of continental crust of 1.9–1.7 Ga age defined by Nd isotopes in the Ketilidian terrain. Contributions to Mineralogy and Petrology 87, 311–318.
Patchett, P.J., Hutchinson, J., Blaxland, A.B., Upton, B.G.J., 1976. Origin of anorthosites, gabbros and potassic ultramafic rocks from the Gardar Province, South Greenland: Sr isotopic ratio studies. Bulletin of the Geological Society of Denmark 25, 79–84.
Pearce, N.J.G., Leng, M.J., 1996. The origin of carbonatites and related rocks from the Igaliko Dyke Swarm, Gardar Province, South Greenland: field, geochemical and C–O–Sr–Nd isotope evidence. Lithos 39, 21–40.
Peng, Z.X., Mahoney, J., Hooper, P., Harris, C., Beane, J., 1994. A role for lower continental crust in flood basalt genesis? Isotopic and incompatible element study of the lower six formations of the western Deccan Traps. Geochimica et Cosmochimica Acta 58, 267–288.
Powell, M., 1978. The crystallisation history of the Igdlerfigssalik nepheline syenite intrusion, Greenland. Lithos 11, 99–120.
Puchtel, I.S., Brügmann, G.E., Hofmann, A.W., 1999. Precise Re–Os mineral isochron and Pb–Nd–Os systematics of a mafic-ultramfic sill in the 2.0 Ga Onega plateau (Baltic Shield). Earth and Planetary Science Letters 170, 447–461.
Puchtel, I.S., Brügmann, G.E., Hofmann, A.W., 2001. ^{187}Os-enriched domain in an Archean mantle plume: evidence from 2.8 Ga komatiites of the Kostomuksha greenstone belt, NW Baltic Shield. Earth and Planetary Science Letters 186, 513–526.
Roddick, J.C., Sullivan, R.W., Dudas, F.Ö., 1992. Precise calibration of Nd tracer isotopic composition for Sm–Nd studies. Chemical Geology 97, 1–8.
Rudnick, R.L., Presper, T., 1990. Geochemistry of intermediate/- to high-pressure granulites. In: Vielzeuf, D., Vidal, P. (Eds.), Granulites and Crustal Evolution. Kluwer Academic Publishing, Dordrecht, pp. 523–550.
Rumble, D., Hoering, T.C., 1994. Analysis of oxygen and sulfur isotope ratios in oxide and sulfide minerals by spot heating with a carbon dioxide laser in a fluorine atmosphere. Accounts of Chemical Research 27, 237–241.
Saal, A.E., Rudnick, R.L., Ravizza, G.E., Hart, S.R., 1998. Re–Os isotope evidence for the composition, formation and age of the lower continental crust. Nature 393, 58–61.
Schmidt, K.H., Bottazzi, P.V.R., Mengel, K., 1999. Trace element partitioning between phlogopite, clinopyroxene and leucite lamproite melt. Earth and Planetary Science Letters 168, 287–299.
Sharp, Z.D., 1990. A laser-based microanalytical method for the in-situ determination of oxygen isotope ratios of silicates and oxides. Geochimica et Cosmochimica Acta 54, 1353–1357.
Shirey, S.B., Walker, R.J., 1998. The Re–Os isotope system in cosmochemistry and high-temperature geochemistry. Annual Review of Earth and Planetary Sciences 26, 423–500.
Spera, F.J., Bohrson, W.A., 2001. Energy-constrained open-system magmatic processes: I. General model and energy-constrained assimilation and fractional crystallization (EC-AFC) formulation. Journal of Petrology 42, 999–1018.
Sproule, R.A., Lambert, D.D., Hoatson, D.M., 2002. Decoupling of the Sm–Nd and Re–Os isotopic systems in sulphid-saturated magmas in the Halls Creek Orogen, Western Australia. Journal of Petrology 43, 375–402.

Stephenson, D., Upton, B.G.J., 1982. Ferromagnesian silicates in a differentiated alkaline complex: Kungnât Fjeld, South Greenland. Mineralogical Magazine 46, 283–300.

Stevenson, R., Upton, B.G.J., Steenfelt, A., 1997. Crust–mantle interaction in the evolution of the Ilimaussaq Complex, South Greenland: Nd isotopic studies. Lithos 40, 189–202.

Sugawara, T., 2000. Empirical relationships between temperature, pressure, and MgO content in olivine and pyroxene saturated liquid. Journal of Geophysical Research 105, 8457–8472.

Tarney, J., Weaver, B.L., 1987. Geochemistry and petrogenesis of Early Proterozoic dyke swarms. In: Halls, H.C., Fahrig, W.C. (Eds.), Mafic Dyke Swarms. Special Publication-Geological Association of Canada, vol. 34, pp. 81–93.

Taylor, H.P., 1980. The effects of assimilation of country rocks by magmas on $^{18}O/^{16}O$ and $^{87}Sr/^{86}Sr$ systematics in igneous rocks. Earth and Planetary Science Letters 47, 243–254.

Taylor, H.P.J., Sheppard, S.M.F., 1986. Igneous rocks: I. Processes of isotopic fractionation and isotope systematics. In: Valley, J.W., Taylor, H.P.J., O'Neil, J.R. (Eds.), Stable IsotopesReviews in Mineralogy, vol. 16, pp. 227–269.

Taylor, P.N., Upton, B.G.J., 1993. Contrasting Pb isotopic compositions in two intrusive complexes of the Gardar magmatic province of South Greenland. Chemical Geology 104, 261–268.

Taylor, P.N., Jones, N.W., Moorbath, S., 1984. Isotopic assessment of relative contributions from crust and mantle sources to the magma genesis of Precambrian granitoid rocks. Philosophical Transactions of the Royal Society of London. A 310, 605–625.

Thompson, R.N., 1981. Thermal aspects of the origin of Hebridean Tertiary acid magmas: I. An experimental study of partial fusion of Lewisian gneisses and Torridonian sediments. Mineralogical Magazine 44, 161–170.

Thompson, R.N., Gibson, S.A., Mitchell, J.G., Dickin, A.P., Leonardos, O.H., Brod, J.A., Greenwood, J.C., 1998. Migrating Cretaceous–Eocene magmatism in the Serra do Mar Alkaline Province, SE Brazil: melts from the deflected Trindade mantle plume? Journal of Petrology 39, 1493–1526.

Toplis, M.J., Carroll, M.R., 1995. An experimental study of the influence of oxygen fugacity on Fe–Ti oxide stability, phase relations, and mineral-melt equilibria in ferro-basaltic systems. Journal of Petrology 36, 1137–1170.

Turner, S.P., Hawkesworth, C.J., Gallagher, K.G., Stewart, K., Peate, D., Mantovani, M., 1996. Mantle plumes, flood basalts and thermal models for melt generation beneath continents: assessment of a conductive heating model. Journal of Geophysical Research 101, 11503–11518.

Upton, B.G.J., 1971. Melting experiments on chilled gabbros and syenogabbros. Carnegie Institute Washington Year Book. Carnegie Institute of Washington, Washington, pp. 112–118.

Upton, B.G.J., Emeleus, C.H., 1987. Mid-Proterozoic alkaline magmatism in southern Greenland: the Gardar Province. In: Fitton, J.G., Upton, B.G.J. (Eds.), The Alkaline Rocks. Special Publication-Geological Society of London, vol. 30, pp. 449–471.

Upton, B.G.J., Thomas, J.E., 1980. The Tugtutôq younger giant dyke complex, South Greenland: fractional crystallisation of transitional olivine basalt magma. Journal of Petrology 21, 167–198.

Upton, B.G.J., Emeleus, C.H., Heaman, L.M., Goodenough, K.M., Finch, A., 2003. Magmatism of the mid-Proterozoic Gardar Province, South Greenland: chronology, petrogenesis and geological setting. Lithos 68, 43–65.

van Bremen, O., Aftalion, M., Allart, J.H., 1974. Isotopic and geochronologic studies on granites from the Ketilidian mobile belt of South Greenland. Bulletin of the Geological Society of America 85, 403–412.

Vennemann, T.W., O'Neil, J.R., 1993. A simple and inexpensive method of hydrogen isotope and water analyses of minerals and rocks based on zinc reagent. Chemical Geology 103, 227–234.

Waight, T., Baker, J., Willigers, B., 2002. Rb isotope dilution analyses by MC-ICPMS using Zr to correct for mass fractionation: towards improved Rb-Sr geochronology? Chemical Geology 186, 99–116.

Walker, R.J., Morgan, J.W., Hanski, E.J., Smolkin, V.F., 1997. Re–Os systematics of Early Proterozoic ferropicrites, Pechenga Complex, northwestern Russia: evidence for ancient ^{187}Os-enriched plumes. Geochimica et Cosmochimica Acta 61, 3145–3160.

Wendt, I., 1986. Radiometrische methoden in der geochronologie-Clausthaler Tektonische Hefte Band, vol. 23. Pilger Verlag, Clausthal-Zellerfeld.

Zheng, Y.-F., 1993. Calculation of oxygen isotope fractionation in anhydrous silicate minerals. Geochimica et Cosmochimica Acta 57, 1079–1091.